ARTICLE

The EB1–Kinesin-14 complex is required for efficient metaphase spindle assembly and kinetochore bi-orientation

Nikolay Kornakov[ID], Bastian Möllers[ID], and Stefan Westermann[ID]

Kinesin-14s are conserved molecular motors required for high-fidelity chromosome segregation, but their specific contributions to spindle function have not been fully defined. Here, we show that key functions of budding yeast Kinesin-14 Cik1-Kar3 are accomplished in a complex with Bim1 (yeast EB1). Genetic complementation of mitotic phenotypes identifies a novel KLTF peptide motif in the Cik1 N-terminus. We show that this motif is one element of a tripartite binding interface required to form a high-affinity Bim1–Cik1-Kar3 complex. Lack of Bim1-binding by Cik1-Kar3 delays cells in mitosis and impairs microtubule bundle organization and dynamics. Conversely, constitutive targeting of Cik1-Kar3 to microtubule plus ends induces the formation of nuclear microtubule bundles. Cells lacking the Bim1–Cik1-Kar3 complex rely on the conserved microtubule bundler Ase1/PRC1 for metaphase spindle organization, and simultaneous loss of plus-end targeted Kar3 and Ase1 is lethal. Our results reveal the contributions of an EB1–Kinesin-14 complex for spindle formation as a prerequisite for efficient kinetochore clustering and bi-orientation.

Introduction

Microtubules are dynamic polymers responsible for chromosome segregation, cell polarity, and intracellular transport in eukaryotes. They are inherently polar structures with a minus end that is usually anchored at a microtubule organizing center (in yeast, the spindle pole body [SPB]) and a dynamic plus end. A number of microtubule-associated proteins regulate microtubule nucleation and dynamic instability properties and promote assembly and organization of individual microtubules into supramolecular structures (Wieczorek et al., 2015; Akhmanova and Steinmetz, 2015).

Kinesin-14s are evolutionarily conserved minus end–directed microtubule motors required for error-free mitosis and meiosis (McDonald and Goldstein, 1990; Walczak et al., 1997; Meluh and Rose, 1990; Cai et al., 2010; Wickstead et al., 2010). Based on in vitro characterization and cellular analysis, different activities of Kinesin-14 motors have been described: they produce minus end–directed motility using an ATP-dependent rotation of the stalk (Endres et al., 2006). With this activity, they can slide microtubules relative to each other in vitro and thus can provide a balancing force against oppositely directed Kinesin-5 motors (Saunders et al., 1997). An extension of this activity is the ATP-dependent sorting of microtubules into parallel bundles

(Braun et al., 2009) or the zippering of antiparallel microtubules during spindle assembly (Hepperla et al., 2014). In addition, yeast Kar3 has been proposed to act as a microtubule depolymerase (Sproul et al., 2005). The motor has been found to copurify with reconstituted centromeric DNA on beads (Middleton and Carbon, 1994), and it has been implicated in lateral kinetochore transport, an intermediate step in sister-chromatid bi-orientation (Tanaka et al., 2007). However, it is unclear which of these proposed activities is critical for mitosis and how it would facilitate chromosome segregation.

Budding yeasts have a single catalytically active Kinesin-14 Kar3 that forms heterodimers with the kinesin-associated protein Cik1 (Fig. 1 A) or Vik1 (Page and Snyder, 1992; Manning et al., 1999; Allingham et al., 2007; Chu et al., 2005). Cik1-Kar3 is required for efficient resolution of syntelic kinetochore-microtubule attachments by an unknown mechanism (Jin et al., 2012). Loss of Cik1-Kar3 function also leads to a delay in cell cycle progression and hypersensitivity to stress agents such as hydroxyurea and elevated temperature (Manning et al., 1999; Liu et al., 2011). We recently reported a novel biochemical activity of Kinesin-14 motors common to several members, including Cik1-Kar3: these molecules have the ability to align a

....

Department of Molecular Genetics, Faculty of Biology, Center of Medical Biotechnology, University of Duisburg-Essen, Essen, Germany.

Correspondence to Stefan Westermann: Stefan.Westermann@uni-due.de.

growing microtubule along an existing one and thereby promote the formation of parallel microtubule bundles from a common microtubule organizing center (Molodtsov et al., 2016). This microtubule "guiding" activity involves an interaction between the motor and the growing plus ends of microtubules via the autonomous plus-end tracker EB1. During this process, the Kinesin-14 motor remains associated with growing plus ends and acts as a compliant cross-linker that promotes the organization of microtubules into bundles. To which extent this activity—and the interaction between Kinesin-14 motors and EB1 in general—is relevant in vivo and how it may contribute to mitotic spindle function in cells has not been tested, partly because separation-of-function mutants that specifically interfere with this activity but leave other aspects of motor function unchanged have not been available.

Here, taking an unbiased approach to defining new molecular elements required for Kinesin-14 function in budding yeast, we show that the mitotic function of Cik1-Kar3 critically requires an interaction with the autonomous plus-end tracker Bim1, and we define the molecular organization of the relevant binding interface. Our results show that the EB1–Kinesin-14 system contributes to key aspects of microtubule organization during metaphase spindle assembly and is therefore a prerequisite for kinetochore bi-orientation and timely progression through mitosis.

Results

Acute depletion of Cik1-Kar3 delays yeast cells in metaphase

To study Kar3 function in yeast cells, we used a conditional depletion system that circumvents the pitfalls of genetic deletions such as adaptations or secondary mutations. To this end, we integrated auxin-inducible degron (AID) tags (Nishimura et al., 2009) at the chromosomal locations of Kar3 and Cik1 and characterized the cellular phenotypes after conditionally depleting the proteins by addition of auxin. Western blotting confirmed that both Cik1 and Kar3 were efficiently depleted within 30 min after auxin addition (Fig. 1 B). Compared with α-factor–arrested cells, which express a short Cik1 isoform lacking the first 35 amino acids, the level of mitotic Cik1 was very low, as described previously (Page and Snyder, 1992; Benanti et al., 2009). In serial dilution assays, the depletion strains displayed similar phenotypes compared with the respective gene deletions (Fig. 1 C). In particular, conditional depletion of Cik1 conferred temperature sensitivity at 37°C, which was partially suppressed by codepleting Kar3. This is consistent with the notion that the phenotypes of Cik1 depletion can partially be attributed to the inappropriate formation of Vik1–Kar3 complexes (Manning et al., 1999). Slow growth may be a consequence of different defects. As Kinesin-14s are involved in chromosome segregation, we suspected that errors in mitosis would be prevented by prolonged activation of the spindle assembly checkpoint, which delays anaphase onset until all chromosomes have bi-oriented. Indeed, conditional depletion of both Cik1 and Kar3 was lethal at 30°C in the absence of the mitotic checkpoint (Fig. 1 D), indicating that these proteins perform important functions before anaphase onset.

To characterize cellular phenotypes after Cik1 depletion, we synchronized cells in a G1-like state by pheromone treatment and released them into a medium containing auxin. We then filmed Cik1-depleted and control cells simultaneously using live-cell fluorescence microscopy to determine the duration of metaphase in individual cells, defined as the time between SPB separation and anaphase onset (Fig. 1 E). We found that the mean metaphase duration of Cik1-depleted cells (46 ± 2 min) was significantly increased compared with control cells (29 ± 1 min).

Closer inspection of spindle length (pole-to-pole distance) and dynamics (change of pole-to-pole distance over time) revealed that Cik1-depleted cells initiated anaphase from a significantly shorter metaphase spindle than control cells (Fig. 1 F). During anaphase, the fast increase in pole-to-pole distance (Phase I) occurred with similar velocity, although Cik1-depleted cells displayed an overall greater variance in anaphase elongation dynamics. We conclude that Cik1 depletion delays anaphase onset and is characterized by a short metaphase spindle, while anaphase phenotypes are relatively mild in comparison.

Cik1 depletion impairs microtubule alignment and kinetochore clustering during metaphase spindle assembly

To define the underlying causes for the shortened metaphase spindle in Cik1-depleted cells, we observed microtubule plus-end markers (Bik1–3xGFP/CLIP-170) and kinetochore markers (Ndc80-GFP) by live-cell microscopy in synchronized cells. Following SPB separation, nuclear Bik1 signals in control cells were typically confined between the two spindle poles. In addition, cytoplasmic Bik1 signals were targeted toward the bud during nuclear migration (Fig. 2 A and Video 1). By contrast, about two thirds of Cik1-depleted cells displayed Bik1 signals that projected away from the spindle axis, indicating severe misalignment of microtubules during spindle assembly. Prior to anaphase onset, Bik1 localization eventually became more confined to the spindle axis also in Cik1-depleted cells (Video 2).

In addition, Ndc80-GFP was followed to determine kinetochore position and bi-orientation in Cik1-AID cells (Fig. 2 B). When control cells were released from α-factor, the Ndc80-GFP signal formed a tight cluster in the vicinity of the SPB. That cluster persisted throughout metaphase and became well separated immediately before anaphase onset, as cells achieved bi-orientation. Throughout the entire process, the Ndc80-GFP signal remained on axis between the two SPBs (0/40 cells with off-axis kinetochores). By contrast, depletion of Cik1 resulted in less tightly clustered Ndc80 immediately after α-factor release. As these cells progressed into mitosis, they separated their spindle poles, but the Ndc80-GFP signal was frequently mispositioned off axis relative to the SPBs (27/40 cells with off-axis kinetochores). Eventually, Cik1-depleted cells also managed to cluster and position Ndc80 on axis between the SPBs, and only after this had occurred were they able to progress into anaphase.

Cik1 depletion impairs microtubule bundle dynamics at the shmoo tip

The small size of the yeast nucleus makes it difficult to assess the dynamics of individual microtubules or organized groups of
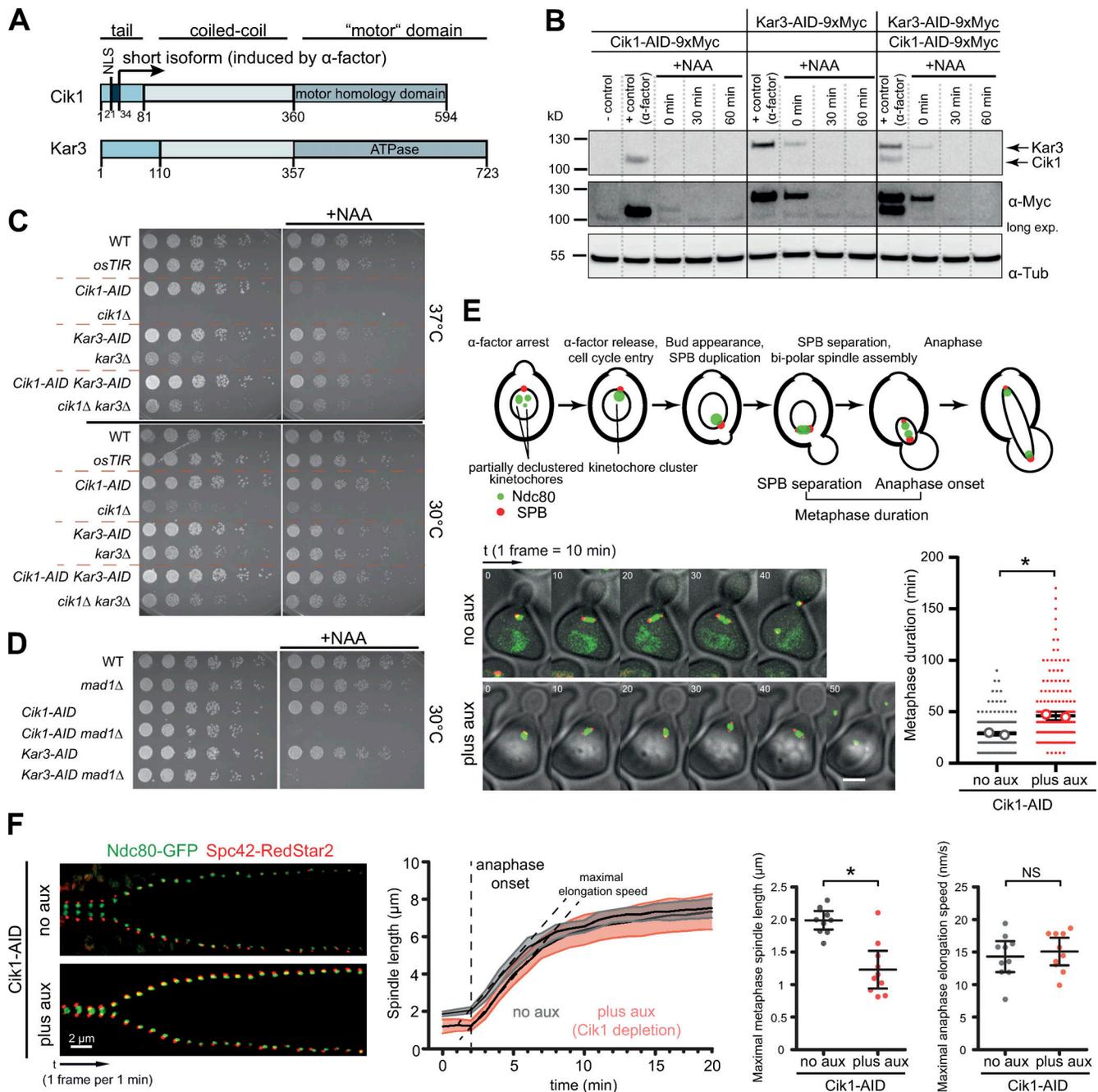
Figure 1. **Depletion of Cik1-Kar3 leads to chromosome mis-segregation and has phenotypes similar to those of knockouts. (A)** Schematic overview of Cik1-Kar3 protein structure. Functionally important regions are highlighted and assigned accordingly. **(B)** Western blot analysis of Cik1-AID and Kar3-AID upon addition of NAA. Kar3 is present in excess over Cik1 in mitotic cells. α-Factor–arrested cells have increased amounts of a shorter Cik1 isoform. Long exp., ong exposure; α-Tub, anti-Tubulin blot. **(C)** Serial dilution spot assays compare *cik1* and *kar3* genetic deletions with the respective conditional depletion alleles. Temperature sensitivity was assayed at 37°C. Plates marked +NAA contained 1 mM of NAA. Plates were incubated for 2.5 d at the stated temperature. **(D)** Analysis of Cik1 or Kar3 depletion in a checkpoint-deficient strain. Plates were incubated for 2.5 d at 30°C. **(E)** Schematic representation of mitotic timing. Metaphase duration is defined as the time between SPB separation and anaphase onset. Gallery of consecutive frames from live-cell imaging of Cik1-AID strains. aux, auxin. The SPB was labeled with Spc42-RedStar2, kinetochores with Ndc80-GFP. Scale bar is 2 μm. Movies are aligned with the separation of SPBs displayed in the first frame. Quantification of metaphase duration in individual Cik1-AID cells. A total of 200 cells from two biological replicates were analyzed. Open circles represent mean duration from each individual experiment; error bars show 95% CI. χ^2 test was applied; *, P < 0.0001. **(F)** Analysis of spindle size and dynamics in Cik1-depleted cells. Left panel: Gallery of consecutive frames from live-cell imaging. Middle and right panels: Quantification of spindle elongation for *n* = 15 cells. Error bars are means with 95% CIs. Student's two-tailed *t* tests were made (*, P < 0.0001; NS, P = 0.59).
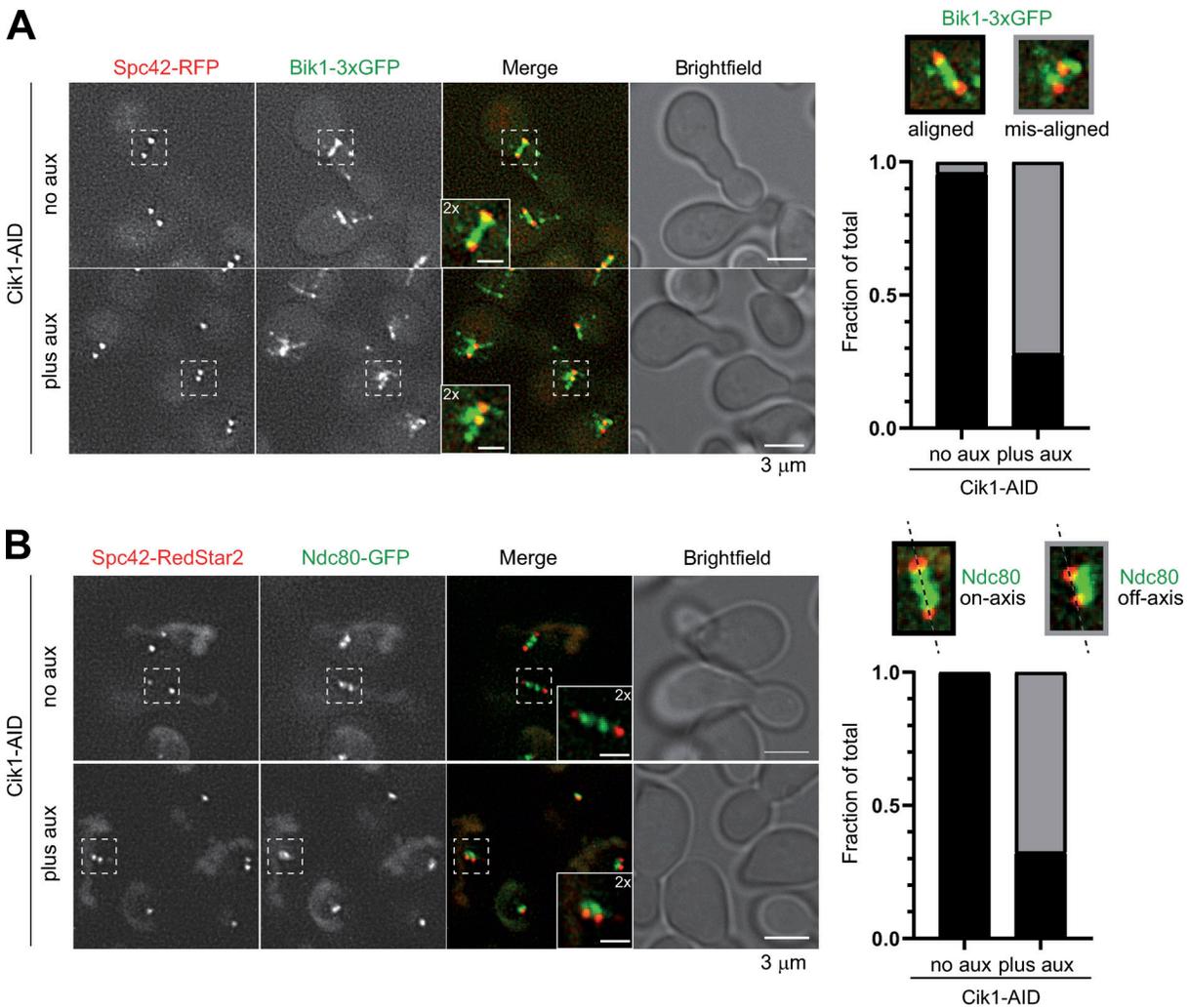
Figure 2. **Cik1 depletion impairs microtubule alignment and kinetochore clustering in metaphase spindles. (A)** Cik1-AID cells expressing the micro-tubule plus-end marker Bik1-3xGFP and the SPB marker Spc42-RFP were imaged in the presence and absence of auxin. Scale bar is 3 µm. Micrograph inserts show 2× magnification of marked spindle. Scale bar is 1 µm. Metaphase spindle morphology in 40 cells was categorized into aligned and misaligned spindles. **(B)** Analysis of kinetochore position in Cik1-depleted cells. Representative fluorescence images of cells expressing the kinetochore marker Ndc80-GFP and the SPB marker Spc42-RedStar2 are shown. Scale bars are 3 µm. Inserts show 2× magnification of a kinetochore cluster together with the SPBs marked by Spc42-RedStar2. Scale bars in the insets are 3 µm. Kinetochore organization in 40 metaphase spindles was categorized into on-axis and off-axis Ndc80 signals relative to the SPBs.

microtubules. We therefore turned to polarized yeast cells, generated by exposure to the mating pheromone α-factor, in which microtubule bundle dynamics can be readily observed by following the movement of the SPB associated with the nuclear membrane. When the microtubule bundle is polymerizing, it pushes the nucleus away from the shmoo tip. Conversely, when the bundle is depolymerizing, it pulls the nucleus toward the shmoo tip (Fig. S1 A). As reported before, Kar3-3xGFP was present as individual dots along the shmoo tip bundle (Molodtsov et al., 2016; Gibeaux et al., 2013), colocalizing with the plus-end marker Stu2 (Fig. S1, B and C). By analyzing ky-mographs of SPB displacement (tagged with Spc42-mCherry) relative to the shmoo tip over time, we quantified microtubule bundle dynamics parameters, as well as microtubule align-ment, in the presence and in the absence of Kar3 (Fig. S1, D and E). We also compared overall bundle dynamics with individual

nuclear microtubules or cytoplasmic microtubules outside the shmoo tip bundle (Fig. S1 F). Interestingly, Kar3 depletion in α-factor–arrested cells affected neither net polymerization nor depolymerization velocity of the bundle (Fig. S1 G) but instead caused microtubule bundle disorganization, with 42/50 ex-amined cells displaying microtubules that failed to align along the SPB-shmoo tip axis. Moreover, the switches between bundle polymerization and depolymerization occurred less frequently in Kar3-depleted cells, causing a 50% increase in time between catastrophes or rescues from 90 s in control to 135 s in Kar3-depleted cells (Δt catastrophe/rescue; Fig. S1 G).

The overall dynamics of microtubule bundles were drasti-cally different from those of individual microtubules, as ana-lyzed by following Stu2-GFP signals, which labeled both polymerizing and depolymerizing plus ends. By obtaining movies with high time resolution, we found that individual

nuclear microtubules had polymerization and depolymerization speeds ~2.4 times faster than those of the microtubule bundle (Fig. S1 F). These observations in α-factor–arrested cells show that Cik1-Kar3 is required to align microtubules into a parallel bundle and to promote frequent switches between overall polymerization and depolymerization of the bundle.

Identification of novel sequence elements required for Cik1-Kar3 function in vivo

We took advantage of the lethality of Cik1 depletion in a *mad1Δ* strain to screen for novel molecular elements required for the mitotic function of Cik1. To this end, Cik1-AID strains were transformed with Cik1 wild type or mutants encoded on centromeric plasmids. To ensure targeting into the nucleus, all constructs contained an SV40 NLS. Viability in the absence of the mitotic checkpoint was scored on plates as a readout for the ability to support error-free chromosome segregation (Fig. 3 A). Since it was previously shown that the C-terminal motor homology domain of Cik1 is required for proper Cik1-Kar3 function (Liu et al., 2011; Mieck et al., 2015), we focused on the contribution of the N-terminal tail. Amino-terminal truncations of increasing size, followed by fine mapping with a resolution of five amino acids, revealed a striking difference between Cik1 variants lacking N-terminal 69 versus 74 residues (Fig. 3 B). While Cik1$^{\Delta 69}$ supported viability upon Cik1 depletion indistinguishable from that of wild-type Cik1, the Cik1$^{\Delta 74}$ mutant was inviable. Multiple sequence alignments of various yeasts revealed that the difference between these Cik1 versions is the presence of a conserved KLTF peptide motif, which is located just N-terminal of a predicted coiled-coil domain in the Cik1 tail (Fig. 3 C).

Since the KLTF peptide motif was specific to Cik1, we asked if placing it into the paralog Vik1 would allow the transfer of critical mitotic Cik1 functions. Overall, Cik1 and Vik1 share a similar organization but display only 20% sequence identity. We generated chimeric constructs in which parts of the Cik1 tail were fused to Vik1 (Fig. 3 D). While full-length Vik1 was unable to rescue the lethality of a Cik1 depletion, chimeric Vik1 constructs containing the Cik1 tail supported viability, but only if these constructs contained the KLTF motif (Vik1-Cik1-Vik1 chimeras VCV1, VCV3, and VCV4). Thus, the key functional difference between the paralogs Cik1 and Vik1 lies in the presence of the KLTF motif, and transferring it to Vik1 allows Vik1 to perform the key mitotic functions otherwise only provided by Cik1 (Fig. 3 D).

We performed a similar complementation analysis for Kar3-AID, focusing on the contribution of the Kar3 N-terminus to mitotic function. This analysis revealed that an internal deletion of residues 89–109 (hereafter termed the ND2 domain) and, within this region more specifically, the deletion of residues 104–108, phenocopied the lack of a rescue allele (Fig. S2, A and B). Interestingly, the identified Kar3 region preceded a predicted coiled-coil domain similar to the corresponding KLTF motif in Cik1, suggesting they might perform a common function.

The Cik1 KLTF motif is a key part of the Bim1-binding interface of Cik1-Kar3

To delineate the molecular function of the KLTF motif in Cik1, we compared the biochemical properties of recombinant Kinesin-14 motors produced in Sf9 insect cells that contained either the Cik1$^{\Delta 69}$ or the Cik1$^{\Delta 74}$ version. Both Cik1 variants were able to form heterodimers with Kar3 (Fig. 4 A) and supported ATP-dependent microtubule motility in vitro (not shown). Since the budding yeast EB1 homologue Bim1 is the only biochemically described binding partner (Mieck et al., 2015), we compared the ability to bind Bim1 in vitro. Strikingly, while Bim1 coeluted with Cik1$^{\Delta 69}$-Kar3 during size exclusion chromatography (SEC), Bim1 binding was abolished for the Cik1$^{\Delta 74}$ variant (Fig. 4 B). We confirmed this result in quantitative pull-down assays, binding soluble motors to increasing amounts of immobilized Bim1 on beads. By quantifying the protein depletion from the supernatant, we estimated an apparent dissociation constant of $K_d \approx 250$ nM for the Cik1$^{\Delta 69}$-Kar3 complex with Bim1, while Cik$^{\Delta 74}$-Kar3 did not display any appreciable affinity (Fig. 4 C). With a dissociation constant in the nanomolar range, the KLTF sequence as part of a novel Bim1-binding motif provides much tighter binding than single EB1-interacting motifs, which have been reported to be in the above micromolar range (Honnappa et al., 2009; Kumar et al., 2017).

A similar biochemical analysis confirmed that the ND2 region in Kar3 also contributes to Bim1 binding in vitro (Fig. S3, A and B). Taken together, our results allow the definition of a composite binding interface between Cik1-Kar3 and Bim1 (Fig. 4 D). This interface is split between Cik1 and Kar3 and consists of two critical parts: first, the ND2 region of Kar3 (motif A), which is necessary but not sufficient to bind Bim1, since it is shared between Vik1–Kar3 and Cik1–Kar3 complexes and Vik1–Kar3 is unable to bind Bim1 (Mieck et al., 2015); and second, the newly identified KLTF peptide motif in Cik1 (motif B), which constitutes the key difference between the Cik1 and Vik1 paralogs. An intact AB-motif is required for high-affinity Bim1 binding. In addition, there is a third, canonical Bim1-binding SxIP motif (Honnappa et al., 2009) at the extreme N-terminus of Cik1 (motif C). This organization is fully consistent with a previously obtained proximity map derived from chemical cross-linking mass spectrometry (XL-MS) experiments (Molodtsov et al., 2016). In particular, Cik1 Lys71 of the "KLTF" motif was found to cross-link to Bim1 Lys223 in the cargo-binding domain. In addition, several cross-links of residues just C-terminal of the KLTF motif with residues in the Bim1 linker- and cargo-binding domain and also to Kar3 ND2 are consistent with the proposed organization (Fig. S4).

Bim1-binding–deficient Cik1 mutants display severe mitotic phenotypes

The definition of the Bim1-binding interface allowed us to construct novel Cik1 mutants defective in the Bim1–Cik1-Kar3 interaction and use these to probe the specific functional contribution of this complex in cells. In particular, we constructed Cik1 mutants in which the Bim1-binding motifs C (SxIP) and B (KLTF) were either mutated individually (to SKNN(AA) or 4A, respectively) or in combination (SKNN(AA)+4A; Fig. 5 A). Using conditional depletion of Cik1-AID in *mad1Δ* cells, we found that the Cik1-SKAA mutant was fully viable, while Cik1-4A displayed slow growth. Combining both mutations in the Cik1–SKAA+4A mutant, however, caused lethality upon Cik1 depletion,
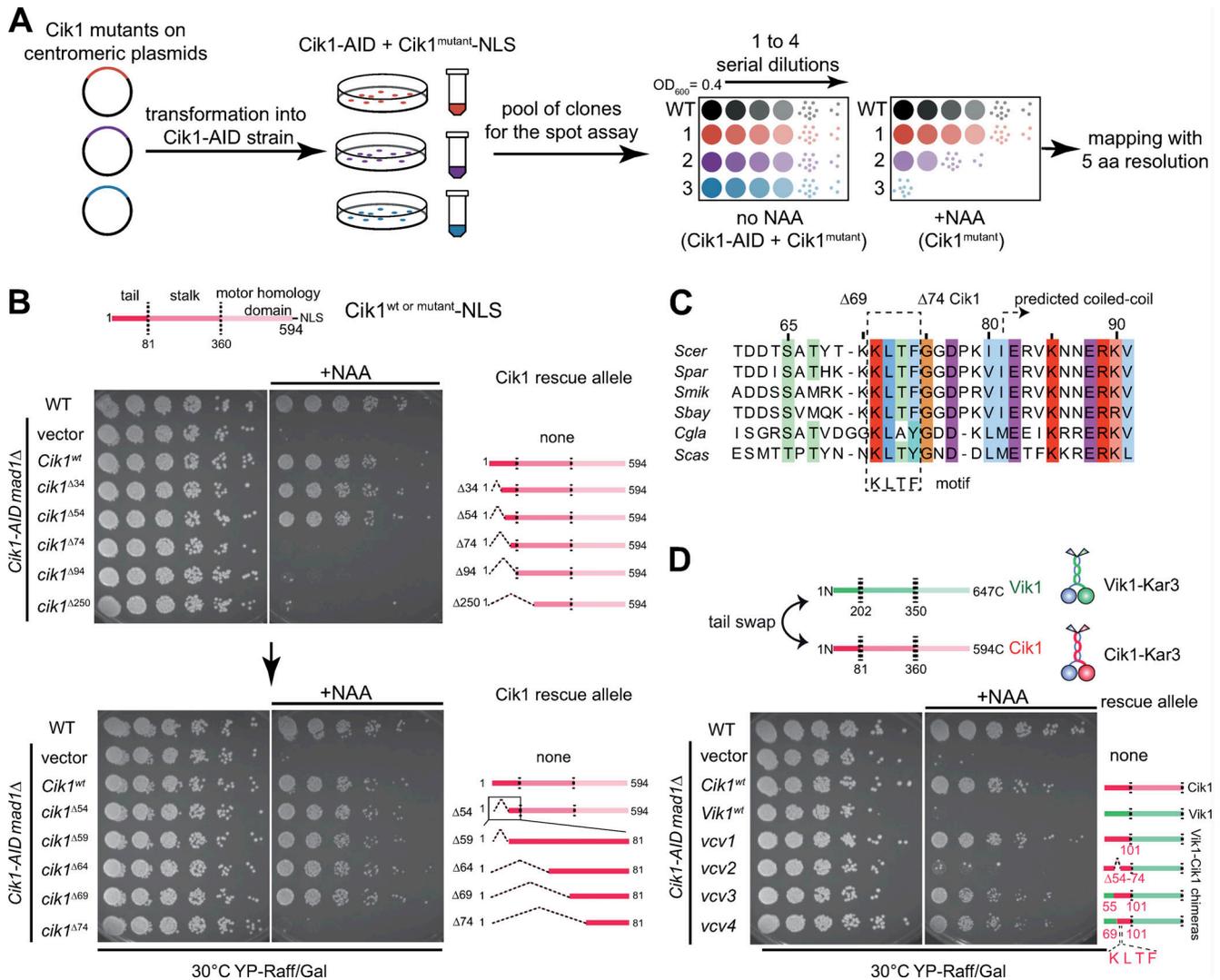
Figure 3. **Molecular dissection of the Cik1 N-terminus reveals a conserved KLTF motif. (A)** Scheme of Cik1 mutagenesis screen. Cik1 mutants were encoded on centromeric plasmids and targeted to the nucleus by an SV40 NLS. After addition of auxin, the only remaining version of Cik1 in the cell was an assayed mutant. **(B)** Subsequent N-terminal truncations of Cik1 allowed to identify a novel functionally important region in the N-terminus. Second panel shows the precise mapping of a region between 54 and 74 aa of Cik1. **(C)** Sequence alignment of Cik1 tail regions from six budding yeast species illustrates a conserved KLTF peptide motif as the difference between Cik1$^{\Delta69}$ and Cik1$^{\Delta74}$. Residues were labeled with the ClustalW coloring scheme in Jalview. **(D)** The KLTF peptide motif defines the key difference between the two kinesin-associated proteins Cik1 and Vik1. Construction of Cik1-Vik1-Cik1 chimeras is shown schematically. Transplantation of the 69–101 aa region, including KLTF, of Cik1 to Vik1 allows the VCV4 (Vik1-Cik1-Vik1) chimera to fulfill Kinesin-14 mitotic functions.

similar to the Cik1$^{\Delta74}$ mutant (Fig. 5 B). Using gene replacements in diploid cells, which also contained a heterozygous deletion of the checkpoint gene *MAD1*, we found that Cik1-4A spores grew poorly, and we failed to recover Cik1-4A spores that also lacked *MAD1* (Fig. 5 C). The Cik1$^{SKNN+4A}$ mutant displayed an even more severe phenotype. The respective spores rarely grew in a wild-type background and were never recovered in a mitotic checkpoint-deficient strain. Analysis of Kar3-3xGFP localization in different cell cycle stages revealed that both Cik1-4A and Cik1$^{SKNN+4A}$ mutants eliminate Kar3 localization to plus ends between the SPBs in both metaphase and anaphase spindles (Fig. S5 A). We confirmed the expression of the different Cik1 alleles by Western blotting (Fig. S5 B). The Cik1-4A mutation also strongly reduced the level of Kar3-3xGFP on the shmoo tip bundle (Fig. S5

C), although some residual colocalization with Stu2 was still visible (Fig. S5 D).

In biochemical experiments, the Cik1-4A mutant eliminated Bim1 interaction during SEC (Fig. S5 E), while it retained some affinity in solid-phase pull-downs. The Cik1–SKAA+4A mutant did not display any affinity for Bim1, even in the pull-down assay, consistent with the most severe phenotypes of this mutant (Fig. S5 F). We used the conditional Cik1-AID system to further characterize the phenotypes of Bim1-binding–deficient Cik1 mutants. Expression of Cik1$^{SKNN+4A}$ led to a checkpoint-dependent accumulation of large-budded cells, similar to those lacking a Cik1 rescue allele (Fig. 5 D). Live-cell imaging further confirmed that expression of wild-type Cik1 rescued the metaphase delay that occurred upon depletion of endogenous Cik1. By
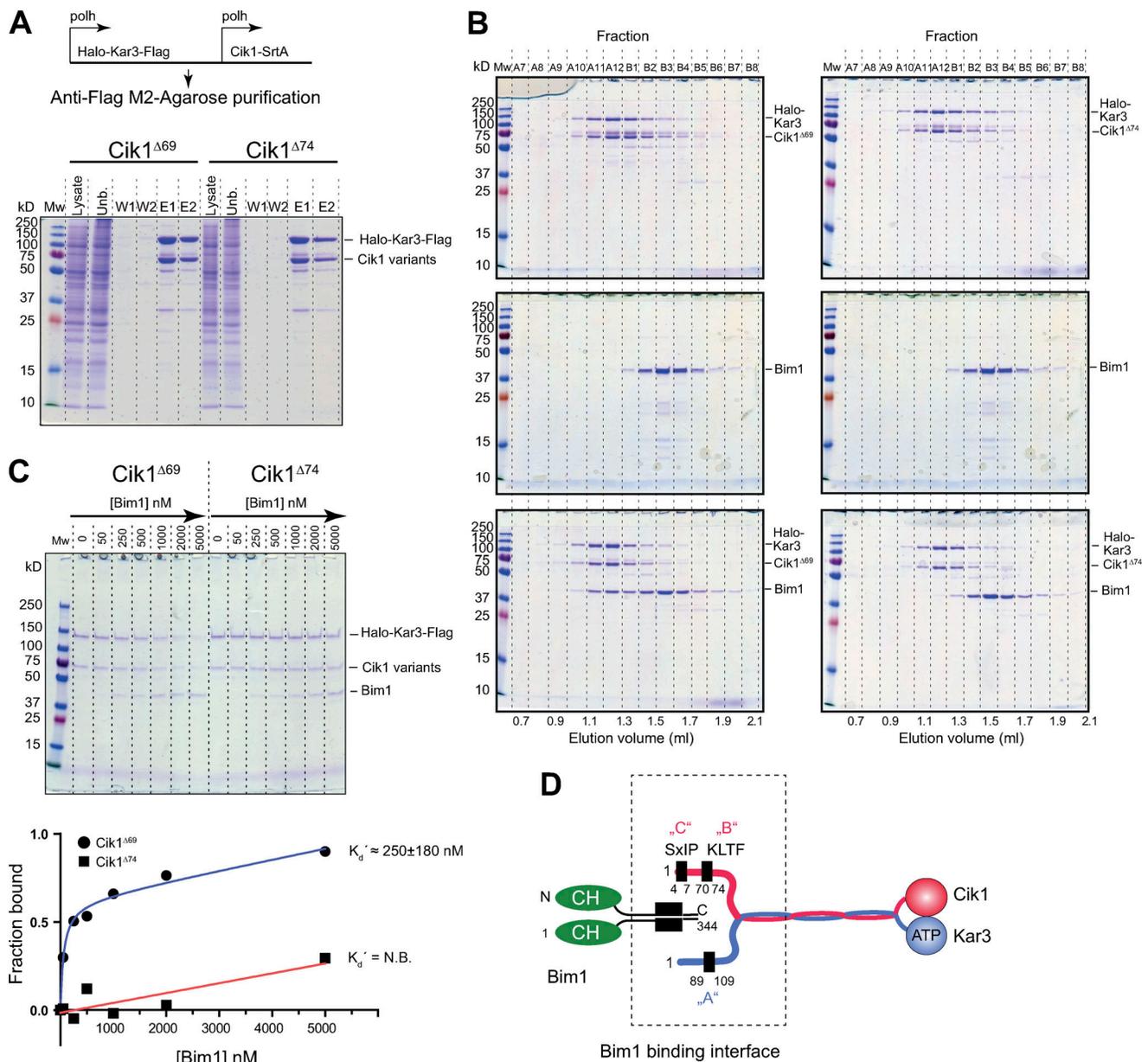
Figure 4. The novel KLTF peptide motif is responsible for high-affinity Bim1 binding by Cik1-Kar3. (A) Purification of Cik1$^{\Delta 69}$-Kar3 and Cik1$^{\Delta 74}$-Kar3. Proteins were eluted from M2-agarose beads with 3xFlag peptide. Gel lanes show Sf9 lysate, unbound fraction (Unb.), wash 1, and wash 2 followed by the two elution fractions E1 and E2. polh, polyhedrin promoter; Mw, molecular weight marker. **(B)** Analysis of Bim1 binding to Cik1$^{\Delta 69}$-Kar3 and Cik1$^{\Delta 74}$-Kar3 in a SEC experiment. Sample fractions from Superose 6 column were resolved on SDS-PAGE and visualized by Coomassie staining. For comparison, the identical Bim1 gel is shown side by side in the middle panel. Input concentration of proteins was 5 µM for the respective Halo–Kar3–Cik1 complex and 10 µM for Bim1. **(C)** Analysis of Bim1 binding in a quantitative pull-down experiment. Representative gel of supernatant fractions from pull-down experiment using Bim1 immobilized on beads incubated with Cik1$^{\Delta 69}$-Kar3 and Cik1$^{\Delta 74}$-Kar3 in solution. Binding is well approximated with the one-site total binding model (smooth line), R^2 = 0.99. Bim1 does not bind to Cik1$^{\Delta 74}$-Kar3 under the given conditions. Experiments were performed at +4°C. Dissociation constant represents mean value of three biological repeats ± SD. N.B., no binding. **(D)** Schematic representation of the binding interface between Cik1-Kar3 and Bim1; the discovered elements of the binding interface are highlighted.

contrast, the Bim1-binding–deficient Cik1$^{SKNN+4A}$ caused an increase in the mean metaphase duration from 31 ± 1 min to 54 ± 3 min (Fig. 5 E). Analysis of spindle dynamics additionally showed that Cik1$^{SKNN+4A}$ cells initiated anaphase from a significantly shorter metaphase spindle (length means ± SEM were 2.14 ± 0.07 µm for Cik1^{WT} and 1.16 ± 0.09 µm for Cik1$^{SKNN+4A}$), while overall anaphase dynamics did not differ strongly from

that of wild-type cells (Fig. 5 G). We conclude that Bim1-binding–deficient Cik1 mutants phenocopy Cik1 depletion, showing that the functionally relevant form of Cik1-Kar3 in yeast cells is its complex with Bim1.

To analyze the impact of the Bim1–Cik1-Kar3 complex on microtubule bundle dynamics in α-factor–arrested cells, we used the Kar3^{ND2} allele, as the Cik1-4A mutant maintained some
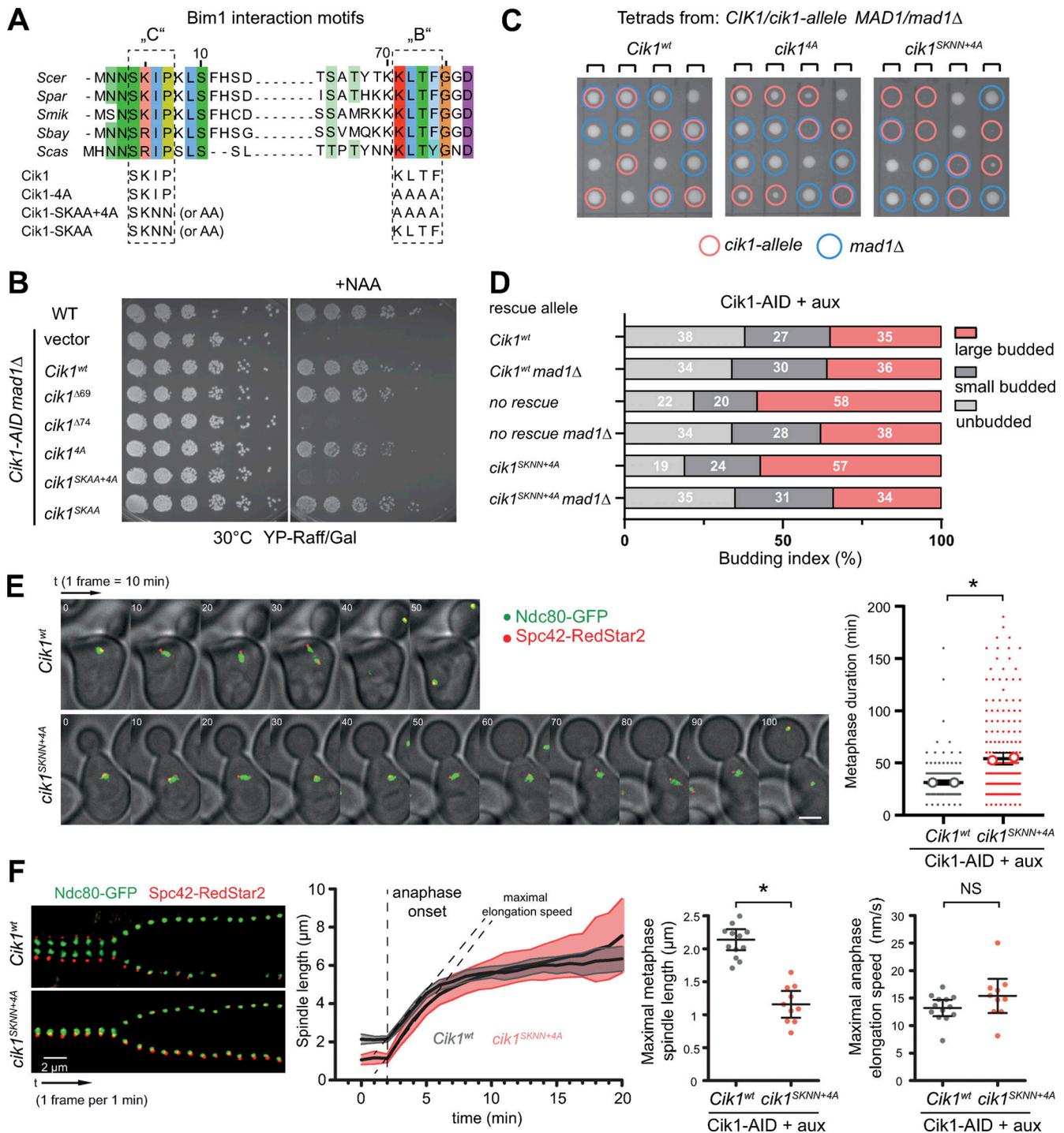
Figure 5. **Bim1–Cik1 interaction mutants display severe mitotic phenotypes. (A)** Scheme of the constructed Bim1–Cik1 interface mutants. Multiple sequence alignment reveals the presence of a conserved canonical EB1 binding motif (SxIP) and the novel KLTF motif. The constructed Cik1 mutants are shown below the alignment. **(B)** Serial dilution assay testing viability of different Cik1 mutants in the Cik1-AID mad1Δ background. **(C)** Heterozygous diploid dissection of different Cik1 alleles in a mad1Δ background. The four spores from an individual tetrad are shown in the respective columns; the indicated gentoypes are marked by circles. Combined mutations in SKIP and KLTF motifs result in a severe growth defect. **(D)** Budding index assay of Cik1-depleted strains expressing the indicated rescue constructs. Log-phase cells were treated with auxin for 3 h. The percentage of the respective cell cycle stage is indicated in white on the graph. Average means of three independent experiments are shown. **(E)** Live-cell microscopy analysis of metaphase duration in Cik1-AID strains expressing a wild-type Cik1 or the Cik1^SKNN+4A allele. Galleries show consecutive frames from live-cell imaging, aligned at the time of SPB separation. Scale bar is 2 μm. Quantification of metaphase duration is from 200 individual cells (two technical repeats). Open circles represent mean duration from each individual experiment. Bars show mean values and 95% CI. χ² test was applied; *, P < 0.0001. **(F)** Analysis of spindle size and dynamics in Cik1-depleted cells expressing either Cik1 wild-type or Cik1^SKNN+4A. Left panel: Gallery of consecutive frames from live-cell imaging. Middle and right panels: Quantification of spindle elongation for n = 15 cells. Error bars are means with 95% CIs. Student's two-tailed t tests were made (*, P < 0.0001; NS, P = 0.14).

plus-end localization of Kar3 (see above). The mutant Kar3, unable to bind Bim1, failed to rescue the decreased frequency between polymerization and depolymerization phases of the shmoo tip bundle, which occurs upon depleting Kar3 (see Fig. S1, C and D), and also caused misalignment of shmoo tip microtubules (Fig. S5 G). We conclude that Cik1-Kar3 function both in mitosis and in α-factor–arrested cells critically requires complex formation with Bim1, which leads to plus-end targeting.

Constitutive plus-end targeting of Cik1-Kar3 restores viability by promoting the alignment of nuclear microtubules
If Bim1 was the only critical interaction partner for Cik1-Kar3, we would predict that constitutive targeting to the microtubule plus end should bypass the molecular requirements for Bim1 binding and restore the mitotic function of the motor. We tested this idea by fusing the N-terminal CH domain of Bim1 (residues 1–133) or of Ndc80 (residues 1–246) directly to the Bim1-binding–deficient Cik1$^{\Delta74}$ mutant (Fig. 6 A). Strikingly, the constructed CH-Cik1 chimeras were capable of supporting viability of *mad1Δ* cells after Cik1 depletion (Fig. 6 B). A corresponding CH-domain fusion to Kar3 failed to rescue the Cik1 depletion, consistent with the notion that Cik1 also contributes to Kar3 function via its motor homology domain (Mieck et al., 2015).

We investigated the effect of the CH-Cik1 chimera on the microtubule cytoskeleton of yeast cells in more detail, specifically by comparing cells that either expressed Bim1-binding–deficient Cik1$^{\Delta74}$-NLS or the fusion protein CH^{Bim1}-Cik1$^{\Delta74}$-NLS. Upon expression of Cik1$^{\Delta74}$-NLS in α-factor–arrested cells, the shmoo tip bundle localization of Kar3 was abolished and Kar3-3xGFP was visible as a diffuse nuclear background signal, which failed to localize to microtubule structures and only showed slight enrichment proximal to the SPB (Fig. 6 C). This confirms that Kar3 localization to the nucleus depends on an NLS normally only present in the mitotic isoform of Cik1 (Benanti et al., 2009). Upon expression of CH-Cik1$^{\Delta74}$–NLS, however, Kar3-3xGFP strongly localized to microtubules emanating as a bundle from the SPB. The nuclear bundle was dynamic, with Kar3-3xGFP appearing as motile spots along the length of the bundle.

We used Bik1-3xGFP to investigate the distribution of plus ends in α-factor–arrested cells. In Cik1 wild-type cells, Bik1 localized prominently to a tightly aligned shmoo tip bundle and displayed weak localization to individual nuclear plus ends (Fig. 6 D). Upon expression of CH-Cik1$^{\Delta74}$–NLS, however, Bik1-3xGFP strongly localized to a nuclear bundle in which individual plus ends were aligned along a common axis. In contrast to this, the shmoo tip bundle in these cells displayed organization defects (Fig. 6 D). Analysis of metaphase duration in individual cells showed that there was no significant difference between Cik1^{WT} and CH-Cik1$^{\Delta74}$–NLS (39 ± 2 min versus 38 ± 2 min, respectively), showing that the fusion protein fully rescued the mitotic timing of Cik1-depleted cells (Fig. 6 E). Just like Cik1$^{\Delta74}$, the Bim1-binding–deficient Kar3^{ND2} mutant could also be rescued by a CH-domain fusion (Fig. 6 F). Microtubule cross-linking and bundle formation via plus-end targeted Kinesin-14s is likely a universal function of these proteins. In line with this notion, we found that the human Kinesin-14 HSET, when fused with the

CH-domain of Bim1 to its tail, was able to complement the depletion of Kar3 in a checkpoint-deficient strain (Fig. 6 G).

Cik1 mutants rely on the microtubule cross-linking protein Ase1/PRC1 for metaphase spindle assembly
While Bim1–Cik1 interaction mutants initially displayed severe microtubule alignment defects, spindle organization eventually improved, and cells were able to enter anaphase with a delay (see Fig. 1 E and Fig. 5 E). To ask how Cik1 mutant cells accomplished spindle assembly, we visualized several other microtubule-binding proteins involved in this process. While we did not detect strong effects on the recruitment of the Kinesin-5 motor Cin8 or the Kinesin-8 Kip3 (data not shown), we noticed that the conserved microtubule bundling protein Ase1/PRC1, which localized only faintly to wild-type metaphase spindles, was significantly enriched on Cik1-depleted or Cik1 mutant spindles (Fig. 7, A and B). Crucially, at the time of anaphase onset, Cik1 mutant spindles contained ~50% more Ase1 than wild-type spindles, as judged by fluorescence microscopy (mean ± SEM). Ase1-3xGFP intensities were 445 ± 14, 606 ± 19, 450 ± 14, and 648 ± 24 a.u. for no auxin, Cik1 depletion, Cik1^{wt}, and Cik1$^{SKNN+4A}$ rescues, respectively (Fig. 7, C and D). If Ase1 recruitment were important for metaphase spindle organization in this context, we would expect synthetic defects between Cik1 and Ase1 mutants. Indeed, codepletion of Cik1 and Ase1 was lethal, even in checkpoint-proficient yeast cells, and viability could be rescued by expression of wild-type Cik1 but not of Bim1-binding–deficient Cik1$^{SKNN+4A}$ (Fig. 7 E). Consistent with the key role for plus-end targeting of Kar3, the CH-Cik1$^{\Delta74}$ fusion was able to rescue the lethality of the Cik1/Ase1 codepletion.

We furthermore investigated the phenotypes of Cik1/Ase1–codepleted cells by live cell microscopy: after addition of auxin, codepleted cells were characterized by a very short spindle, whose length was decreased relative to that of Cik1-depleted cells or of Cik1/Ase1–codepleted cells rescued by a Cik1 wild-type construct (representing the effect of the individual Ase1 depletion; Fig. 7 F; means ± SEM spindle lengths were 1.65 ± 0.02, 0.97 ± 0.01, 1.26 ± 0.02, and 0.93 ± 0.01 µm for no auxin, plus aux, Cik1^{wt}, and Cik1$^{SKNN+4A}$, respectively). Visualizing microtubule plus ends with Bik1-3xGFP in this strain revealed that codepleted cells had a highly abnormal spindle morphology characterized by severe microtubule alignment defects, with most of the nuclear Bik1 fluorescence localized away from the pole-to-pole axis (Fig. 7 G). We conclude that lack of Kar3 plus-end targeting and simultaneous depletion of Ase1 prevent the assembly of a functional metaphase spindle.

Discussion
Here, we define the molecular basis for the formation of a complex between EB1 and Kinesin-14 in budding yeast and analyze the contribution of this complex to spindle organization and function. The definition of the binding interface allowed us to construct highly specific point mutants that avoid complications that arise from interpreting phenotypes of deletion mutants. A Cik1 deletion mutant, for example, will not only prevent the formation of Cik1–Kar3 complexes but will also change the

Kornakov et al.
Spindle assembly requires EB1–Kinesin-14 complex

Journal of Cell Biology   9 of 17
https://doi.org/10.1083/jcb.202003072
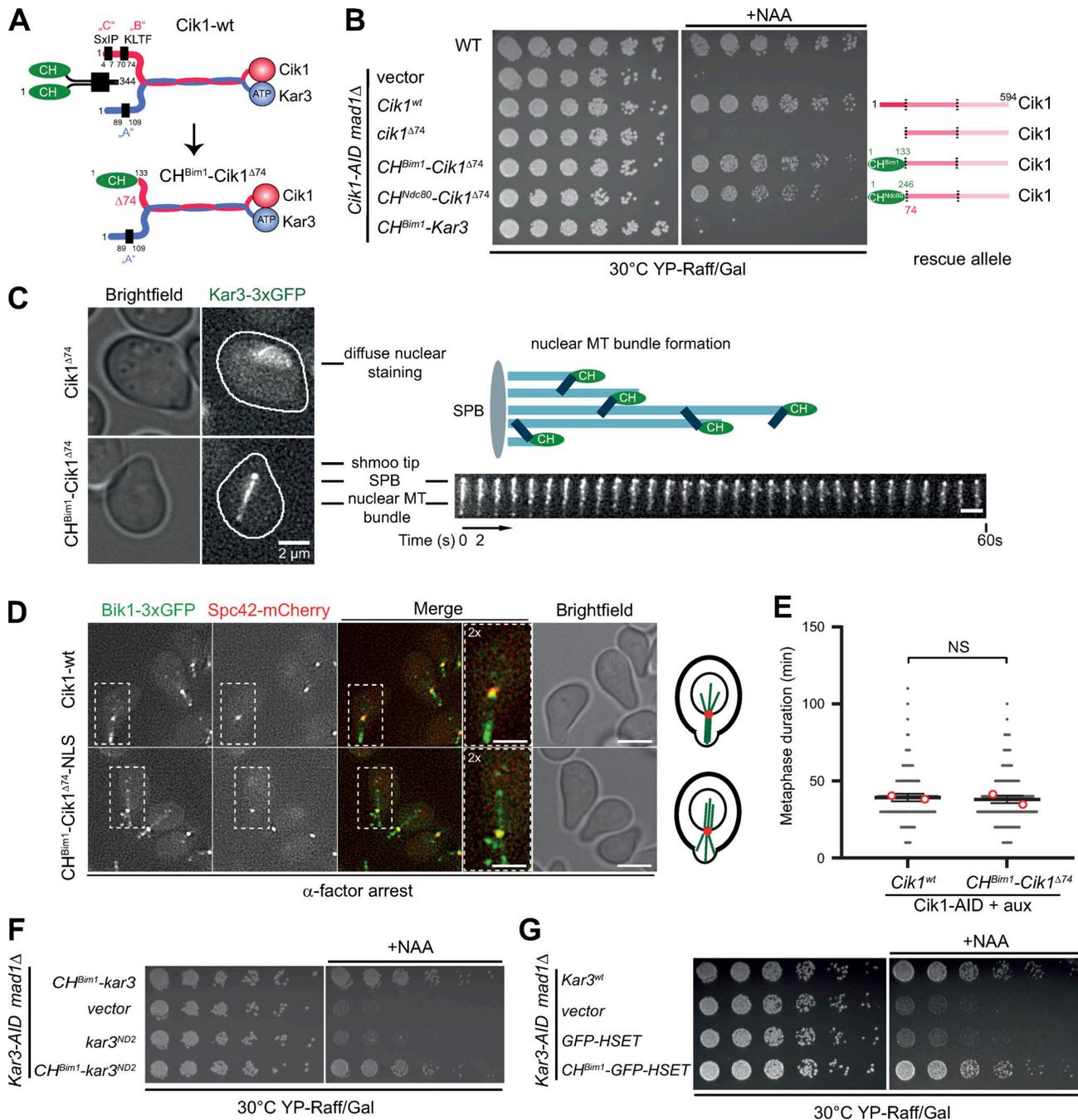
Figure 6. **Artificial targeting of Cik1-Kar3 to the plus end is sufficient to induce nuclear bundle formation and restore viability in the absence of a checkpoint.** (A) Cartoon describing the construction of the CH^{Bim1}-Cik1$^{\Delta74}$ construct. The CH domain of Bim1 (residues 1–133) was fused to a Cik1 mutant that lacks Bim1 binding. (B) Serial dilution assay of different Cik1 alleles in the Cik1-AID *mad1Δ* strain background. (C) Analysis of Kar3 localization in Bim1-binding–deficient Cik1$^{\Delta74}$ or CH^{Bim1}-Cik1$^{\Delta74}$ cells during an α-factor arrest. Scale bar is 2 μm. Montage on the right side shows 30 consecutive frames with 2-s time interval of the nuclear microtubule bundle in the CH^{Bim1}-Cik1$^{\Delta74}$ strain. Scale bar is 2 μm. (D) Fluorescence micrographs of α-factor–arrested Cik1 wild-type or CH^{Bim1}-Cik1$^{\Delta74}$-NLS cells expressing the plus-end marker Bik1-3xGFP and Spc42 mCherry. Scale bar is 4 μm. Insert shows 2× magnification of the indicated area. Scale bar is 2 μm. Cartoon on the right depicts organization of the microtubule cytoskeleton. (E) Quantification of metaphase duration in Cik1-AID cells treated with auxin and expressing either Cik1 wild-type (39 ± 2 min) or CH^{Bim1}-Cik1$^{\Delta74}$-NLS (38 ± 2 min). 160 and 170 cells, respectively, were quantified from two technical repeats. Open circles represent mean duration from each individual experiment. Bars denote 95% CIs. χ^2 test was applied; NS, P > 0.9999. (F) A CH-domain fusion rescues the growth defect of the Bim1-binding–deficient Kar3^{ND2} mutant. Serial dilution assay of the indicated strains in a Kar3-AID *mad1Δ* strain background. (G) A CH-domain fusion to human Kinesin-14 HSET can rescue the lethality of the Kar3 depletion in a checkpoint-deficient strain.
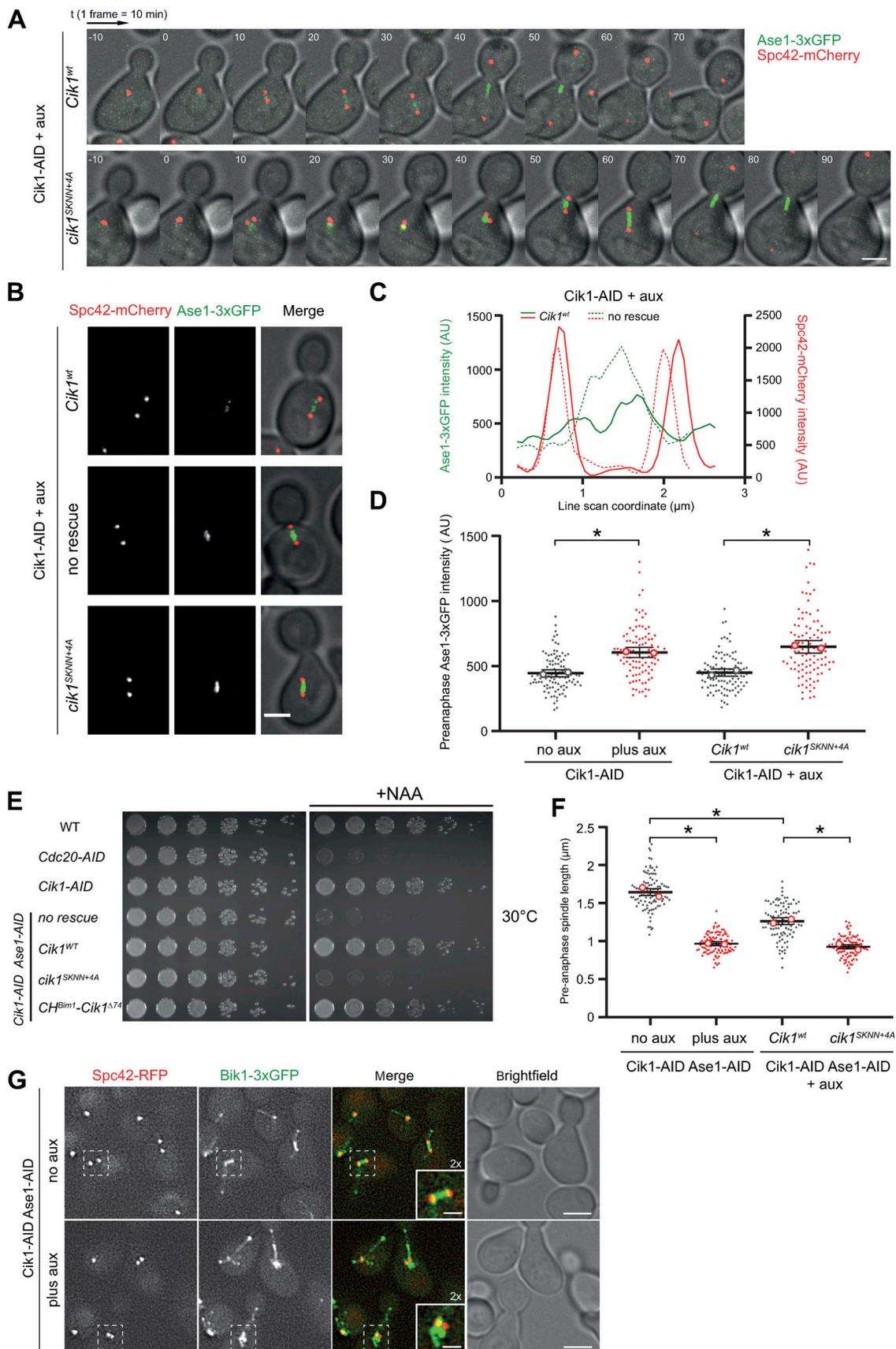
Figure 7. Bim1–Cik1 interaction mutants rely on the conserved microtubule cross-linker Ase1/PRC1 for metaphase spindle assembly. (A) Live-cell imaging of Ase1 recruitment to Cik1 wild-type or Cik1$^{SKNN+4A}$ mutant cells. Consecutive frames from live-cell movies are displayed, aligned to the time of SPB

separation. Scale bar is 2 µm. **(B)** Fluorescence micrographs showing Ase1 recruitment to metaphase spindles. Equally intensity-scaled fluorescence micrographs are shown. Scale bar is 3 µm. **(C)** Line scan profile quantifying Ase1-3xGFP on metaphase spindles in Cik1-AID cells treated with auxin and containing either Cik1 wild-type or no rescue allele. **(D)** Quantification of Ase1-3xGFP intensity on pre-anaphase spindles under the indicated conditions. 100 cells were analyzed for each condition from two technical repeats. Open circles represent mean intensity from each individual experiment. Bars denote 95% CI. Kruskal-Wallis test was done; *, P < 0.0001. **(E)** Simultaneous depletion of Cik1 and Ase1 is analyzed by a serial dilution assay of the indicated strains on YP-Raff/Gal at 30°C in the absence and presence of auxin. Cdc20-AID is included as a control for the depletion of an essential protein. **(F)** Quantification of pre-anaphase spindle length in the indicated strains. 100 cells were analyzed for each condition from two technical repeats. Bars denote 95% CI. Kruskal-Wallis test was done; *, P < 0.0001. Difference between plus aux and Cik1$^{SKNN+4A}$ was not significant. **(G)** Fluorescence microscopy of Cik1-AID Ase1-AID codepleted cells expressing the microtubule plus-end marker Bik1-3xGFP. Scale bar is 3 µm. Inserts are 2× magnifications of the indicated areas. Scale bar is 1 µm.

amount of Vik1–Kar3 complexes in the cell (our unpublished data). In addition, the N-terminal domains of Cik1 and Kar3 encode a number of other functionalities, such as nuclear localization signals or degron sequences (Benanti et al., 2009). The discovery of the KLTF motif in Cik1 is another example of short binding motifs that are present in addition to—or instead of—the well-documented SxIP motifs in EB1 cargos (Kumar et al., 2017). It will be interesting to see whether different binding modes reflect different functionalities of EB1–cargo complexes. In some cases, the EB1 interaction may simply be used for local enrichment of the cargo at the microtubule plus end; in other cases, however, the EB1–cargo complex may perform a joint biochemical function, requiring a high-affinity interaction. The EB1–Kinesin-14 complex seems to be an example for the latter mode of action.

We show that a key biochemical activity of the EB1–Kinesin-14 complex is its ability to convert highly dynamic individual microtubules into bundles, while at the same time promoting the overall ability of the bundle to switch between polymerization and depolymerization. Our results show that microtubule alignment by the Bim1–Cik1-Kar3 complex contributes to building a dynamic metaphase spindle on which sister chromatid bi-orientation can occur efficiently. We propose that the EB1–Kinesin-14 complex contributes to this process via multiple different mechanisms (Fig. 8):

First, bundle formation contributes to early spindle assembly and microtubule alignment, consistent with previously reported phenotypes for a *cik1Δ* strain (Hepperla et al., 2014). The reduced size of the metaphase spindle and the mispositioned kinetochores that we observed upon Cik1 depletion or in the Bim1-interaction mutants are consistent with this interpretation. Our results show, however, that these functions of Cik1-Kar3 are accomplished as a complex with Bim1 at the microtubule plus end, suggesting that the type of antiparallel zippering proposed by Gardner and colleagues (Hepperla et al., 2014), which would include Bim1-independent translocation along microtubules, may provide only a secondary contribution. We rather favor the idea that parallel bundles generated by Bim1–Cik1-Kar3 from both SPBs serve as optimized binding sites with sufficient overlap for Kinesin-5 motors whose role in early spindle formation was described recently (Leary et al., 2019).

Second, bundle formation contributes to the spatial organization of yeast kinetochores into SPB-proximal clusters (Jin et al., 2000). This type of organization may facilitate the bi-orientation process, and there is evidence for coordinated movements between different pericentromeres, suggesting that they behave as a single unit (Stephens et al., 2013). In this

way, Bim1–Cik1-Kar3 can contribute to the organization of a half-spindle as a kinetochore fiber that links to 16 individual kinetochores, thus resembling the organization of bundle attachments to a single kinetochore in higher eukaryotes (Nixon et al., 2015; Vukušić et al., 2017). In higher eukaryotes, plus end–directed motors such as CENP-E make important contributions to kinetochore congression during prometaphase (Kapoor et al., 2006), while microtubule bundle organization also requires nucleation of new microtubules via the Augmin complex (Petry et al., 2013; David et al., 2019), which is absent in yeast. These distinct functional requirements may reflect differences in dimension and organization between different types of mitotic spindles.

Third, the high density of microtubules in the spindle provided by tight bundling through Bim1–Cik1-Kar3 allows the generation of a sufficient number of accessible binding surfaces for kinetochores to effectively switch between lateral and end-on attachments during the error correction process (Kalantzaki et al., 2015). In addition, the Bim1–Cik1-Kar3 complex promotes frequent transitions of the microtubule bundle between polymerization and depolymerization, thus ensuring that it is dynamic. This activity is best exemplified at the shmoo tip bundle, where depletion of Cik1-Kar3 makes the bundle less dynamic without affecting the speed of polymerization or depolymerization. The frequent switches are important for the quality control of kinetochore–microtubule interactions, as the error correction process requires repeated attempts to generate tension across the kinetochore structure (Suzuki et al., 2016; Tanaka et al., 2002). Consequently, tubulin mutants that display reduced dynamics also delay bi-orientation (Huang and Huffaker, 2006). By promoting microtubule bundle dynamics, Bim1–Cik1-Kar3 supports Ipl1 kinase (Aurora B) in the resolution of syntelic attachments (Tanaka et al., 2002). More direct roles for Kar3 in lateral kinetochore transport, as suggested from experiments using a CEN-reactivation system (Tanaka et al., 2007), are probably not making a substantial contribution to bi-orientation during regular mitosis, or at least our genetic analysis argues that they could only be secondary to the Bim1-provided plus-end function of the complex.

We further show that Cik1 mutant cells rely on the conserved microtubule–cross-linker Ase1 for successful metaphase spindle assembly. Given the pronounced defects in microtubule alignment and overlap in Bim1–Cik1 interaction mutants, it was surprising that Ase1 nevertheless accumulated on these misorganized spindles. We envision at least two possible explanations for this effect. First, the prolonged metaphase arrest may simply give Ase1 more time to associate with metaphase spindles.

spindle organization

kinetochore bi-orientation

alignment

metaphase spindle

wild-type

efficient bi-orientation

Cik1 Δ74 or
Cik1 SKNN+4A

disrupted
EB1-Kinesin-14
complex

increased Ase1

delay

shorter spindle

delayed bi-orientation

disrupted
EB1-Kinesin-14
complex
+
Ase1 depletion

delay

very short spindle

monotelic
attachments

syntelic
attachments

insufficient anti-parallel overlap
failure to bi-orient

Kinesin-14-EB1 complex

PRC1

MT plus-end

CH

CH

Bim1

sister chromatids

Kar3-Cik1-Bim1

Ase1

Cik1-Kar3

Figure 8. **Model for the role of the EB1–Kinesin-14 complex during spindle function.** Schematic description of spindle assembly and kinetochore bi-orientation in wild-type cells (top row), cells with a disrupted EB1–Kinesin 14 complex (middle row), and simultaneous loss of EB1–Kinesin-14 and Ase1/PRC1 (bottom row). Left side depicts effects on spindle microtubule organization. Right side describes consequences for sister chromatid bi-orientation. Please see Discussion for details.

Alternatively, the lack of plus end–targeted Kar3 may liberate binding sites on the metaphase spindle previously inaccessible to Ase1. Wild-type cells limit the accumulation of Ase1 on the spindle via phosphorylation in order to prevent premature sliding of interpolar MTs in metaphase (Khmelinskii et al., 2009). In the Cik1 mutant situation, however, Ase1 recruitment appears to be beneficial, and simultaneous loss of plus end–targeted Kar3 and Ase1 yields spindles that manage to separate SPBs but cannot generate sufficient microtubule alignment and anti-parallel overlap to allow kinetochore bi-orientation (Fig. 8). This is consistent with recent studies demonstrating that the initial step in the monopolar-to-bipolar transition is driven by Kinesin-5–based cross-linking (Leary et al., 2019). Our results indicate, however, that despite the

presence of Kinesin-5, plus-end targeted Kinesin-14 and Ase1 are critically required for the maturation of the nascent metaphase spindle into a properly organized scaffold for kinetochores to bi-orient. Previously, Ase1 phenotypes have mostly been described affecting anaphase spindle elongation (Khmelinskii et al., 2007). Synthetic defects observed with a conditional Cin8 depletion, however, are consistent with the idea that Ase1 also makes important contributions to metaphase spindle assembly (Kotwaliwale et al., 2007). In the same context, fission yeast Ase1 is required for spindle assembly in the absence of opposing Kinesin-5 and -14 motors (Rincon et al., 2017), and it collaborates with Kinesin-14 for the generation of bipolar microtubule bundles in the cytoplasm (Janson et al., 2007).

Overall, our study identifies microtubule organization by the EB1–Kinesin-14 complex as an important prerequisite for efficient chromosome bi-orientation. Future research will have to address how the successive action of multiple motors, bundlers, and plus-end trackers is coordinated and how bundle dynamics within the spindle are regulated on a molecular level.

Materials and methods

Yeast genetics
All used strains were derived by modification of the wild-type strains DDY1102, DDY902, and DDY904 (S288c background; Table S1). Genetic modifications were performed by standard LiAc transformation using homologous recombination (Janke et al., 2004; Longtine et al., 1998). Yeasts were generally maintained in YPD medium. For protein depletion experiments, yeasts were grown in YEP medium/plates with raffinose and galactose (YP-Raff/Gal) as a sugar source at 30°C unless otherwise stated.

Preparation of Cik1-AID and Kar3-AID strains
The Ubiquitin ligase osTIR1 was integrated into the URA3 locus under the control of a galactose-inducible promoter (Nishimura et al., 2009). Cik1 and Kar3 were C-terminally tagged at their genomic loci with AID-9xMyc by integration of a corresponding PCR product. Successful integrations were verified by sequencing. Depletion was achieved by adding 1 mM auxin (NAA) to the medium/plates.

Gene deletion and tagging
Target genes were deleted or tagged using PCR products amplified from plasmid libraries. Deletions were confirmed by PCRs for the absence of the wild-type gene and the presence of a selection marker at the correct genomic loci.

Western blot sample preparation
Yeast cell extracts were prepared using alkaline treatment as described before (Kushnirov, 2000). Briefly, the equivalent of 2 OD_{600} of exponentially growing cells was harvested, washed with H_2O, and resuspended in 200 µl 0.1 M NaOH. After 5-min incubation at room temperature, cells were centrifuged again. The pellet was resuspended in 50 µl 1× SDS sample buffer and boiled for 5 min. 8–10 µl lysate was loaded per gel lane.

Used antibodies and visualization
Antibodies used were α-GFP (Roche; from mouse, catalog no. 11814460001) 1:1,000; α-myc (Covance; 9E10 from mouse, catalog no. MMS-150R) 1:1,000; α-PGK 1:10,000 (Invitrogen; from mouse, catalog no. 459250); α-Flag M2-HRP (Sigma; from mouse, catalog no. A 8592) 1:10,000; α-tubulin-HRP 1:1,000 (Santa Cruz; from rat, catalog no. sc-53030); and HRP-coupled α-mouse (GE Healthcare; catalog no. NA931) 1:10,000. All antibodies were diluted in 5% (wt/vol) milk in Tris-buffered saline containing 0.01% (vol/vol) Tween-20.

For visualization Amersham ECL Prime Western Blotting Detection Reagent (GE Healthcare) was used. Images were acquired by Amersham Imager 600 (GE Healthcare).

Plasmid construction
All plasmids generated and used are listed in Table S2. For generation of protein–protein fusions overlapping, PCR was routinely used. Mutations were usually introduced by whole-plasmid amplification using overlapping primers followed by in-bacteria recombination, similar to what was described (Xia et al., 2015). Constructs for insect cell expression were cloned into pLIB and pBig1a plasmids using Gibson assembly as described before (Weissmann and Peters, 2018).

Recombinant protein expression and purification
Cik1–Kar3 complexes and HSET constructs were expressed from recombinant baculoviruses in Sf9 insect cells, cultivated in Spodopan (Pan Biotech) media for 3 d after infection. At that time point, 80–90% of cells were positive for a GFP reporter construct. Cells were collected by centrifugation, and the pellet was frozen in liquid nitrogen and stored at –80°C until further use. Proteins were purified as described before (Molodtsov et al., 2016). Briefly, cells were lysed using a Dounce homogenizer, and proteins were purified using M2–anti-Flag agarose. Lysis buffer contained 25 mM Hepes-KOH, pH 7.4, 150 mM NaCl, 1 mM $MgCl_2$, 5% (wt/vol) glycerol, 0.1% (vol/vol) Tween-20, 0.5 mM Tris(2-carboxyethyl)phosphin (TCEP), 0.5 mM ATP, 0.1 mM PMSF, and protease and phosphatase inhibitors (Roche). After washing, proteins were eluted with 2 mg/ml of 3xFlag peptide dissolved in 25 mM Hepes-KOH pH, 7.4, 150 mM NaCl, 1 mM $MgCl_2$, 5% (wt/vol) glycerol, 0.1% (vol/vol) Tween-20, and 0.5 mM TCEP buffer and stored at –80°C.

Bim1 and EB1 were expressed in *Escherichia coli* Rosetta cells and purified by Ni-NTA affinity chromatography via a His_6-tag in Lysis buffer containing 300 mM NaCl. After purification, proteins were desalted, and the tag was cleaved off by incubation with Tobacco Etch Virus protease overnight at +4°C. Proteins were loaded onto a Superdex 200 column as a second purification step.

SEC
Analytical SEC runs were performed at 4°C in buffer containing 25 mM Hepes-KOH, pH 7.4, 150 mM NaCl, 1 mM $MgCl_2$, 5% (wt/vol) glycerol, 0.1% (vol/vol) Tween-20, and 0.5 mM TCEP. Superose 6 3.2/300 or Superdex 200 3.2/300 columns were used. Protein complexes were used at 5-µM input concentration for the motor complexes and 10-µM input concentration for Bim1. 100-µl fractions were collected in 96-well plates, and aliquots were analyzed by SDS-PAGE.

Quantitative Bim1 pull-downs
His_6-Bim1 was coupled to prewashed TALON beads in SEC buffer supplemented with 10 mM imidazole and 0.5 mg/ml of BSA at 4°C for 1 h. Beads were washed four times and resuspended in a desired volume. The suspension was added to recombinant Cik1-Kar3, and to allow binding, the mixture was incubated at 4°C for 1 h with rotation. Afterward, beads were collected by centrifugation, and aliquots of the supernatant were analyzed by SDS-PAGE. Coomassie-stained protein bands were quantified in ImageJ/Fiji. Curve fit assumes one-site total binding, which includes specific binding and a linear nonspecific binding

Kornakov et al.
Spindle assembly requires EB1–Kinesin-14 complex

Journal of Cell Biology   14 of 17
https://doi.org/10.1083/jcb.202003072

component: $Y = B_{max} * X/(K_d + X) + NS * X + Background$, where Y is total binding, X is ligand, K_d is dissociation constant, NS is the slope of unspecific binding, and B_{max} is the maximum specific binding.

Live-cell fluorescence microscopy
Quantification of mitotic timing and spindle phenotypes
For protein depletion experiments, cells were grown for 18–20 h in YEPRG (2% of raffinose and 0.2% of galactose, vol/vol) and diluted to 0.1–0.2 OD_{600} in YEPRG. Cells were allowed to achieve exponential growth for 3 h at 30°C. Then, 0.01 mg/ml of α-factor was added for 2 h to arrest cells in a G1-like state.

Synchronized cells were collected by centrifugation, and α-factor was washed away with prewarmed media three times. The second wash contained pronase. For protein depletion, the third wash contained 1 mM NAA. After the last wash, cells were resuspended in drop-out tryptophan minimal media with Raff/Gal as a sugar source. For protein depletion experiments, 1 mM NAA was kept in all media during all steps. Cells were immobilized on Concanavalin A–coated ibidi Glass Bottom 4 Well μ-Slide 1.5H and proceeded for imaging. Live-cell microscopy was performed at 30°C using the DeltaVison Elite wide-field microscope system (GE Healthcare) equipped with a scientific CMOS camera. A 100× objective (Olympus; NA = 1.40) and immersion oil with a refractive index of $n = 1.518$ were used. Images were acquired by optical axis integration (OAI) scans over 3-μm width. Usually, images were taken every 10 min. Kinetochore clustering was evaluated by connecting the SPBs with a line of 10-pixel width and quantifying off-axis (mispositioned) versus on-axis (correctly positioned) KTsubunit–GFP signal.

Quantification of microtubule dynamics
Individual dynamics of nuclear microtubules were measured in α-factor–arrested cells by following the Stu2-GFP signal. OAI scans were taken every 2 s. To quantify shmoo tip bundle dynamics, short (2-min) and long (5-min) movies were recorded. In the short movies, a z-stack was recorded every 5 s, whereas the time between two z-stacks in the longer movies was 10 s. z-Stacks had 3-μm width, with 0.3-μm spacing between imaging planes.

Image processing
All images were deconvolved using SoftWoRx 7 (options: enhanced ratio, aggressive); image analysis was performed using ImageJ/Fiji software.

Statistical analysis
Statistical tests and graphs were prepared using Graphpad Prism 8. Small points on graphs show values of individual cells, and large open circles represent means of biological or technical replicates, as indicated. 95% confidence intervals (CIs) are usually shown. In the text, mean values ± SEM are mentioned. Student's t test was used to compare continuous data from two strains. Due to small sample size, data distribution was assumed to be normal, but this was not formally tested. The Kruskal-Wallis test was applied to datasets with more than two mutants. For discrete data, the χ^2 test was used.

Online supplemental material
Fig. S1 shows characterization of the Kar3 depletion phenotype on microtubule bundle dynamics in α-factor–arrested yeast cells, related to Fig. 1. Fig. S2 shows genetic identification of key molecular elements in Kar3, related to the corresponding Cik1 analysis in Fig. 3. Fig. S3 shows biochemical analysis of the Kar3[ND2] mutant. Fig. S4 displays chemical cross-linking data illustrating the organization of the Bim1-Cik1-Kar3 interface. Fig. S5 shows additional characterization of Bim1-binding–deficient Cik1 mutants, as well as characterization of the Kar3[ND2] mutant. Video 1 shows microtubule plus ends labeled with Bik1-3xGFP (green) and SPBs labeled with Spc42-RFP (red) in Cik1-AID cells over the course of a synchronized cell cycle under control conditions. Video 2 shows Bik1-3xGFP and Spc42-RFP upon depletion of Cik1-AID. Note misorganization of microtubule plus ends on the nascent metaphase spindle at t = 10 min. Table S1 lists yeast strains used in this study. Table S2 lists the relevant plasmids used in this study.

Acknowledgments

References
Akhmanova, A., and M.O. Steinmetz. 2015. Control of microtubule organization and dynamics: two ends in the limelight. *Nat. Rev. Mol. Cell Biol.* 16:711–726. https://doi.org/10.1038/nrm4084

Allingham, J.S., L.R. Sproul, I. Rayment, and S.P. Gilbert. 2007. Vik1 modulates microtubule-Kar3 interactions through a motor domain that lacks an active site. *Cell.* 128:1161–1172. https://doi.org/10.1016/j.cell.2006.12.046

Benanti, J.A., M.E. Matyskiela, D.O. Morgan, and D.P. Toczyski. 2009. Functionally distinct isoforms of Cik1 are differentially regulated by APC/C-mediated proteolysis. *Mol. Cell.* 33:581–590. https://doi.org/10.1016/j.molcel.2009.01.032

Braun, M., D.R. Drummond, R.A. Cross, and A.D. McAinsh. 2009. The kinesin-14 Klp2 organizes microtubules into parallel bundles by an

ATP-dependent sorting mechanism. *Nat. Cell Biol.* 11:724–730. https://doi.org/10.1038/ncb1878

Cai, S., L.N. Weaver, S.C. Ems-McClung, and C.E. Walczak. 2010. Proper organization of microtubule minus ends is needed for midzone stability and cytokinesis. *Curr. Biol.* 20:880–885. https://doi.org/10.1016/j.cub.2010.03.067

Chu, H.M.A., M. Yun, D.E. Anderson, H. Sage, H.-W. Park, and S.A. Endow. 2005. Kar3 interaction with Cik1 alters motor structure and function. *EMBO J.* 24:3214–3223. https://doi.org/10.1038/sj.emboj.7600790

David, A.F., P. Roudot, W.R. Legant, E. Betzig, G. Danuser, and D.W. Gerlich. 2019. Augmin accumulation on long-lived microtubules drives amplification and kinetochore-directed growth. *J. Cell Biol.* 218:2150–2168. https://doi.org/10.1083/jcb.201805044

Endres, N.F., C. Yoshioka, R.A. Milligan, and R.D. Vale. 2006. A lever-arm rotation drives motility of the minus-end-directed kinesin Ncd. *Nature.* 439:875–878. https://doi.org/10.1038/nature04320

Gibeaux, R., A.Z. Politi, F. Nédélec, C. Antony, and M. Knop. 2013. Spindle pole body-anchored Kar3 drives the nucleus along microtubules from another nucleus in preparation for nuclear fusion during yeast karyogamy. *Genes Dev.* 27:335–349. https://doi.org/10.1101/gad.206318.112

Hepperla, A.J., P.T. Willey, C.E. Coombes, B.M. Schuster, M. Gerami-Nejad, M. McClellan, S. Mukherjee, J. Fox, M. Winey, D.J. Odde, et al. 2014. Minus-end-directed Kinesin-14 motors align antiparallel microtubules to control metaphase spindle length. *Dev. Cell.* 31:61–72. https://doi.org/10.1016/j.devcel.2014.07.023

Honnappa, S., S.M. Gouveia, A. Weisbrich, F.F. Damberger, N.S. Bhavesh, H. Jawhari, I. Grigoriev, F.J.A. van Rijssel, R.M. Buey, A. Lawera, et al. 2009. An EB1-binding motif acts as a microtubule tip localization signal. *Cell.* 138:366–376. https://doi.org/10.1016/j.cell.2009.04.065

Huang, B., and T.C. Huffaker. 2006. Dynamic microtubules are essential for efficient chromosome capture and biorientation in S. cerevisiae. *J. Cell Biol.* 175:17–23. https://doi.org/10.1083/jcb.200606021

Janke, C., M.M. Magiera, N. Rathfelder, C. Taxis, S. Reber, H. Maekawa, A. Moreno-Borchart, G. Doenges, E. Schwob, E. Schiebel, et al. 2004. A versatile toolbox for PCR-based tagging of yeast genes: new fluorescent proteins, more markers and promoter substitution cassettes. *Yeast.* 21:947–962. https://doi.org/10.1002/yea.1142

Janson, M.E., R. Loughlin, I. Loïodice, C. Fu, D. Brunner, F.J. Nédélec, and P.T. Tran. 2007. Crosslinkers and motors organize dynamic microtubules to form stable bipolar arrays in fission yeast. *Cell.* 128:357–368. https://doi.org/10.1016/j.cell.2006.12.030

Jin, Q.W., J. Fuchs, and J. Loidl. 2000. Centromere clustering is a major determinant of yeast interphase nuclear organization. *J. Cell Sci.* 113:1903–1912.

Jin, F., H. Liu, P. Li, H.-G. Yu, and Y. Wang. 2012. Loss of function of the Cik1/Kar3 motor complex results in chromosomes with syntelic attachment that are sensed by the tension checkpoint. *PLoS Genet.* 8. e1002492. https://doi.org/10.1371/journal.pgen.1002492

Kalantzaki, M., E. Kitamura, T. Zhang, A. Mino, B. Novák, and T.U. Tanaka. 2015. Kinetochore-microtubule error correction is driven by differentially regulated interaction modes. *Nat. Cell Biol.* 17:421–433. https://doi.org/10.1038/ncb3128

Kapoor, T.M., M.A. Lampson, P. Hergert, L. Cameron, D. Cimini, E.D. Salmon, B.F. McEwen, and A. Khodjakov. 2006. Chromosomes can congress to the metaphase plate before biorientation. *Science.* 311:388–391. https://doi.org/10.1126/science.1122142

Khmelinskii, A., C. Lawrence, J. Roostalu, and E. Schiebel. 2007. Cdc14-regulated midzone assembly controls anaphase B. *J. Cell Biol.* 177:981–993. https://doi.org/10.1083/jcb.200702145

Khmelinskii, A., J. Roostalu, H. Roque, C. Antony, and E. Schiebel. 2009. Phosphorylation-dependent protein interactions at the spindle midzone mediate cell cycle regulation of spindle elongation. *Dev. Cell.* 17:244–256. https://doi.org/10.1016/j.devcel.2009.06.011

Kotwaliwale, C.V., S.B. Frei, B.M. Stern, and S. Biggins. 2007. A pathway containing the Ipl1/aurora protein kinase and the spindle midzone protein Ase1 regulates yeast spindle assembly. *Dev. Cell.* 13:433–445. https://doi.org/10.1016/j.devcel.2007.07.003

Kumar, A., C. Manatschal, A. Rai, I. Grigoriev, M.S. Degen, R. Jaussi, I. Kretzschmar, A.E. Prota, R. Volkmer, R.A. Kammerer, et al. 2017. Short Linear Sequence Motif LxxPTPh Targets Diverse Proteins to Growing Microtubule Ends. *Structure.* 25:924–932.E4. https://doi.org/10.1016/j.str.2017.04.010

Kushnirov, V.V. 2000. Rapid and reliable protein extraction from yeast. *Yeast.* 16:857–860. https://doi.org/10.1002/1097-0061(20000630)16:9<857::AID-YEA561>3.0.CO;2-B

Leary, A., S. Sim, E. Nazarova, K. Shulist, R. Genthial, S.K. Yang, K.H. Bui, P. Francois, and J. Vogel. 2019. Successive Kinesin-5 Microtubule Cross-linking and Sliding Promote Fast, Irreversible Formation of a Stereotyped Bipolar Spindle. *Curr. Biol.* 29:3825–3837.E3. https://doi.org/10.1016/j.cub.2019.09.030

Liu, H., F. Jin, F. Liang, X. Tian, and Y. Wang. 2011. The Cik1/Kar3 motor complex is required for the proper kinetochore-microtubule interaction after stressful DNA replication. *Genetics.* 187:397–407. https://doi.org/10.1534/genetics.110.125468

Longtine, M.S., A. McKenzie, III, D.J. Demarini, N.G. Shah, A. Wach, A. Brachat, P. Philippsen, and J.R. Pringle. 1998. Additional modules for versatile and economical PCR-based gene deletion and modification in Saccharomyces cerevisiae. *Yeast.* 14:953–961. https://doi.org/10.1002/(SICI)1097-0061(199807)14:10<953::AID-YEA293>3.0.CO;2-U

Manning, B.D., J.G. Barrett, J.A. Wallace, H. Granok, and M. Snyder. 1999. Differential regulation of the Kar3p kinesin-related protein by two associated proteins, Cik1p and Vik1p. *J. Cell Biol.* 144:1219–1233. https://doi.org/10.1083/jcb.144.6.1219

McDonald, H.B., and L.S.B. Goldstein. 1990. Identification and characterization of a gene encoding a kinesin-like protein in Drosophila. *Cell.* 61:991–1000. https://doi.org/10.1016/0092-8674(90)90064-L

Meluh, P.B., and M.D. Rose. 1990. KAR3, a kinesin-related gene required for yeast nuclear fusion. *Cell.* 60:1029–1041. https://doi.org/10.1016/0092-8674(90)90351-E

Middleton, K., and J. Carbon. 1994. KAR3-encoded kinesin is a minus-end-directed motor that functions with centromere binding proteins (CBF3) on an in vitro yeast kinetochore. *Proc. Natl. Acad. Sci. USA.* 91:7212–7216. https://doi.org/10.1073/pnas.91.15.7212

Mieck, C., M.I. Molodtsov, K. Drzewicka, B. van der Vaart, G. Litos, G. Schmauss, A. Vaziri, and S. Westermann. 2015. Non-catalytic motor domains enable processive movement and functional diversification of the kinesin-14 Kar3. *eLife.* 4. e04489. https://doi.org/10.7554/eLife.04489

Molodtsov, M.I., C. Mieck, J. Dobbelaere, A. Dammermann, S. Westermann, and A. Vaziri. 2016. A Force-Induced Directional Switch of a Molecular Motor Enables Parallel Microtubule Bundle Formation. *Cell.* 167:539–552.E14. https://doi.org/10.1016/j.cell.2016.09.029

Nishimura, K., T. Fukagawa, H. Takisawa, T. Kakimoto, and M. Kanemaki. 2009. An auxin-based degron system for the rapid depletion of proteins in nonplant cells. *Nat. Methods.* 6:917–922. https://doi.org/10.1038/nmeth.1401

Nixon, F.M., C. Gutiérrez-Caballero, F.E. Hood, D.G. Booth, I.A. Prior, and S.J. Royle. 2015. The mesh is a network of microtubule connectors that stabilizes individual kinetochore fibers of the mitotic spindle. *eLife.* 4. e07635. https://doi.org/10.7554/eLife.07635

Page, B.D., and M. Snyder. 1992. CIK1: a developmentally regulated spindle pole body-associated protein important for microtubule functions in Saccharomyces cerevisiae. *Genes Dev.* 6:1414–1429. https://doi.org/10.1101/gad.6.8.1414

Petry, S., A.C. Groen, K. Ishihara, T.J. Mitchison, and R.D. Vale. 2013. Branching microtubule nucleation in Xenopus egg extracts mediated by augmin and TPX2. *Cell.* 152:768–777. https://doi.org/10.1016/j.cell.2012.12.044

Rincon, S.A., A. Lamson, R. Blackwell, V. Syrovatkina, V. Fraisier, A. Paoletti, M.D. Betterton, and P.T. Tran. 2017. Kinesin-5-independent mitotic spindle assembly requires the antiparallel microtubule crosslinker Ase1 in fission yeast. *Nat. Commun.* 8:15286. https://doi.org/10.1038/ncomms15286

Saunders, W., V. Lengyel, and M.A. Hoyt. 1997. Mitotic spindle function in Saccharomyces cerevisiae requires a balance between different types of kinesin-related motors. *Mol. Biol. Cell.* 8:1025–1033. https://doi.org/10.1091/mbc.8.6.1025

Sproul, L.R., D.J. Anderson, A.T. Mackey, W.S. Saunders, and S.P. Gilbert. 2005. Cik1 targets the minus-end kinesin depolymerase kar3 to microtubule plus ends. *Curr. Biol.* 15:1420–1427. https://doi.org/10.1016/j.cub.2005.06.066

Stephens, A.D., C.E. Snider, J. Haase, R.A. Haggerty, P.A. Vasquez, M.G. Forest, and K. Bloom. 2013. Individual pericentromeres display coordinated motion and stretching in the yeast spindle. *J. Cell Biol.* 203:407–416. https://doi.org/10.1083/jcb.201307104

Suzuki, A., B.L. Badger, J. Haase, T. Ohashi, H.P. Erickson, E.D. Salmon, and K. Bloom. 2016. How the kinetochore couples microtubule force and centromere stretch to move chromosomes. *Nat. Cell Biol.* 18:382–392. https://doi.org/10.1038/ncb3323

Tanaka, T.U., N. Rachidi, C. Janke, G. Pereira, M. Galova, E. Schiebel, M.J.R. Stark, and K. Nasmyth. 2002. Evidence that the Ipl1-Sli15 (Aurora

kinase-INCENP) complex promotes chromosome bi-orientation by altering kinetochore-spindle pole connections. *Cell*. 108:317–329. https://doi.org/10.1016/S0092-8674(02)00633-5

Tanaka, K., E. Kitamura, Y. Kitamura, and T.U. Tanaka. 2007. Molecular mechanisms of microtubule-dependent kinetochore transport toward spindle poles. *J. Cell Biol*. 178:269–281. https://doi.org/10.1083/jcb.200702141

Vukušić, K., R. Buđa, A. Bosilj, A. Milas, N. Pavin, and I.M. Tolić. 2017. Microtubule Sliding within the Bridging Fiber Pushes Kinetochore Fibers Apart to Segregate Chromosomes. *Dev. Cell*. 43:11–23.E6. https://doi.org/10.1016/j.devcel.2017.09.010

Walczak, C.E., S. Verma, and T.J. Mitchison. 1997. XCTK2: a kinesin-related protein that promotes mitotic spindle assembly in Xenopus laevis egg extracts. *J. Cell Biol*. 136:859–870. https://doi.org/10.1083/jcb.136.4.859

Weissmann, F., and J.-M. Peters. 2018. Expressing Multi-subunit Complexes Using biGBac. *Methods Mol. Biol*. 1764:329–343. https://doi.org/10.1007/978-1-4939-7759-8_21

Wickstead, B., K. Gull, and T.A. Richards. 2010. Patterns of kinesin evolution reveal a complex ancestral eukaryote with a multifunctional cytoskeleton. *BMC Evol. Biol*. 10:110. https://doi.org/10.1186/1471-2148-10-110

Wieczorek, M., S. Bechstedt, S. Chaaban, and G.J. Brouhard. 2015. Microtubule-associated proteins control the kinetics of microtubule nucleation. *Nat. Cell Biol*. 17:907–916. https://doi.org/10.1038/ncb3188

Xia, Y., W. Chu, Q. Qi, and L. Xun. 2015. New insights into the QuikChange™ process guide the use of Phusion DNA polymerase for site-directed mutagenesis. *Nucleic Acids Res*. 43. e12. https://doi.org/10.1093/nar/gku1189

Supplemental material

G

		V_{pol}, nm/s	V_{depol}, nm/s	Δt_{cat}, s	Δt_{rescue}, s	pause duration, s	%, paused
	individual MT	37.7±8.9	77.7±18.7	N.A.	N.A.	N.A.	N.A.
bundle	wt	15.5±1.7	29.2±4.4	89.4±0.3	89.9±1.1	22.5±0.6	7.6
	Kar3-AID — no NAA	15.9±2.3	30.1±5.3	93.9±10.7	91.4±15.1	23.9±5.2	6.5
	Kar3-AID — +NAA	17.2±3.3	35.2±5.7	127.2±1.4	133.4±6.5	36.4±5	8.9
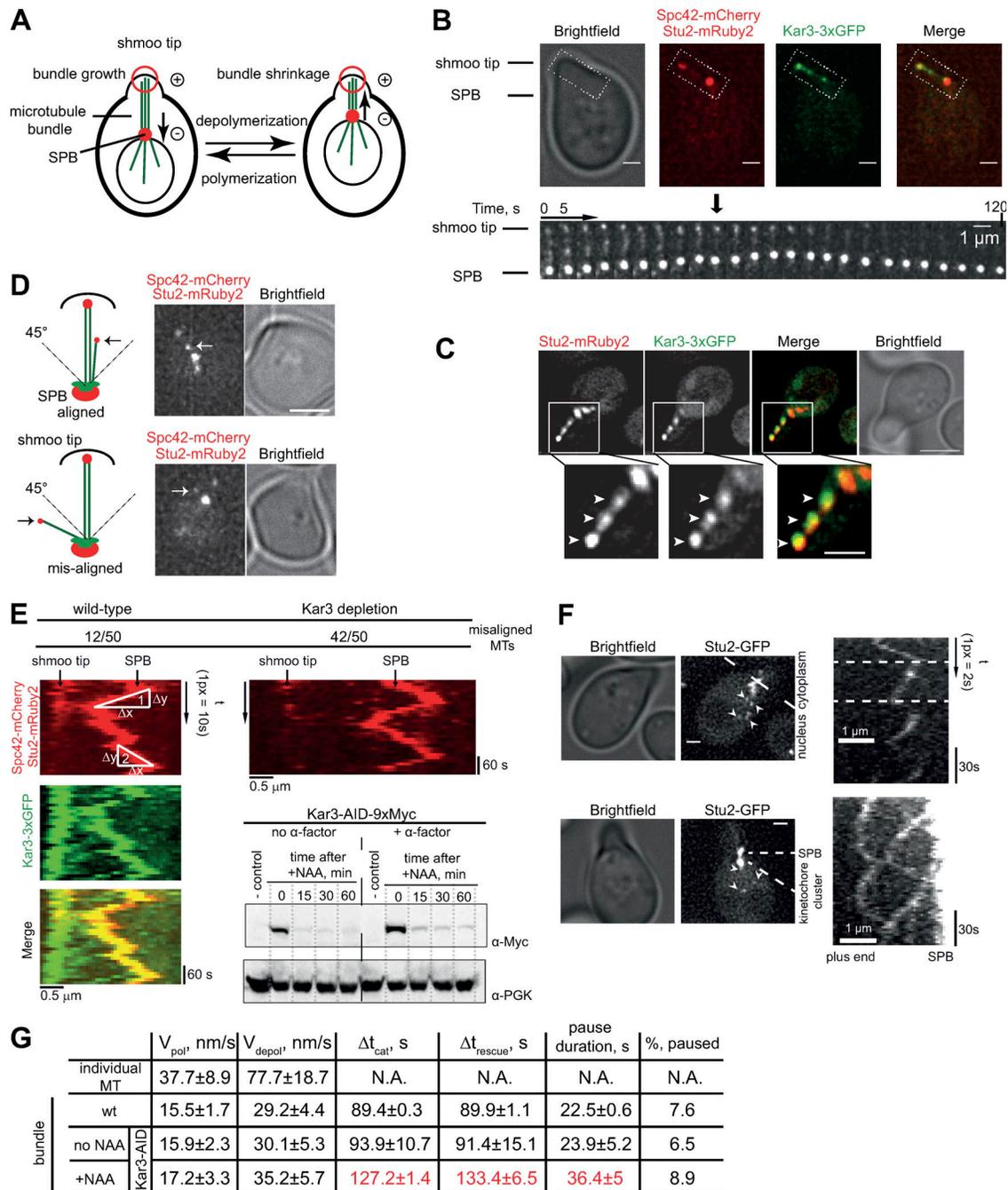
Figure S1. **Cik1-Kar3 promotes shmoo tip microtubule bundle dynamics without affecting polymerization and depolymerization speed. (A)** Diagram describing microtubule bundle dynamics in an α-factor–arrested cell. Cycles of bundle shrinkage and growth cause pulling and pushing of the nucleus toward and away from the shmoo tip. **(B)** Representative image of a polarized cell. The dotted white rectangle includes the microtubule bundle between the shmoo tip and the SPB. Below, a montage of the area is shown; 25 consecutive frames with 5-s time intervals. Scale bar is 1 µm. **(C)** Fluorescence micrographs showing colocalization of Kar3 and Stu2 to individual plus ends (depicted by arrowheads) in the shmoo tip bundle. Scale bar is 2 µm; in magnified inset, scale bar is 1 µm. **(D)** Examples for scoring for shmoo tip alignment defects. Bundle was scored as misaligned when growing Stu2-mRuby2 comets deviated >45° from the SPB to the shmoo tip axis. Arrows point to aligned versus misaligned microtubules. Scale bar is 2 µm. **(E)** Kymographs from a 5-min-long movie of a wild-type and Kar3-AID + NAA cell are shown. The triangles show Δx and Δy as an example for how bundle dynamics values were acquired (1 = depolymerization; 2 = polymerization). Number of cases when at least one microtubule was misaligned during movie acquisition is shown above the kymographs. Scale bars are 0.5 µm. Immunoblotting shows time course and efficiency of Kar3-AID depletion after addition of 1 mM NAA in exponentially growing and α-factor–arrested cells. α-PGK, anti-Phospho-glycerol kinase blot as loading control. **(F)** Individual nuclear microtubules are highly dynamic. α-Factor–arrested cells expressing Stu2-GFP were followed by live-cell microscopy. Arrowheads point to individual microtubule plus ends. Kymographs from 2-min high time-resolution movies of Stu2-GFP. Upper panel shows a single individual microtubule; bottom panel has several microtubules replacing each other. Dashed lines show one polymerization cycle. Scale bar is 1 µm. **(G)** Parameters of dynamics of individual microtubules (top row) and MT bundles (three bottom rows) are listed in the table. pol, polymerization; depol, depolymerization; cat, catastrophe. Parameters that differ from others are highlighted in red. Experiments were repeated at least three times, and means ± SD are shown. N.A., nonapplicable.
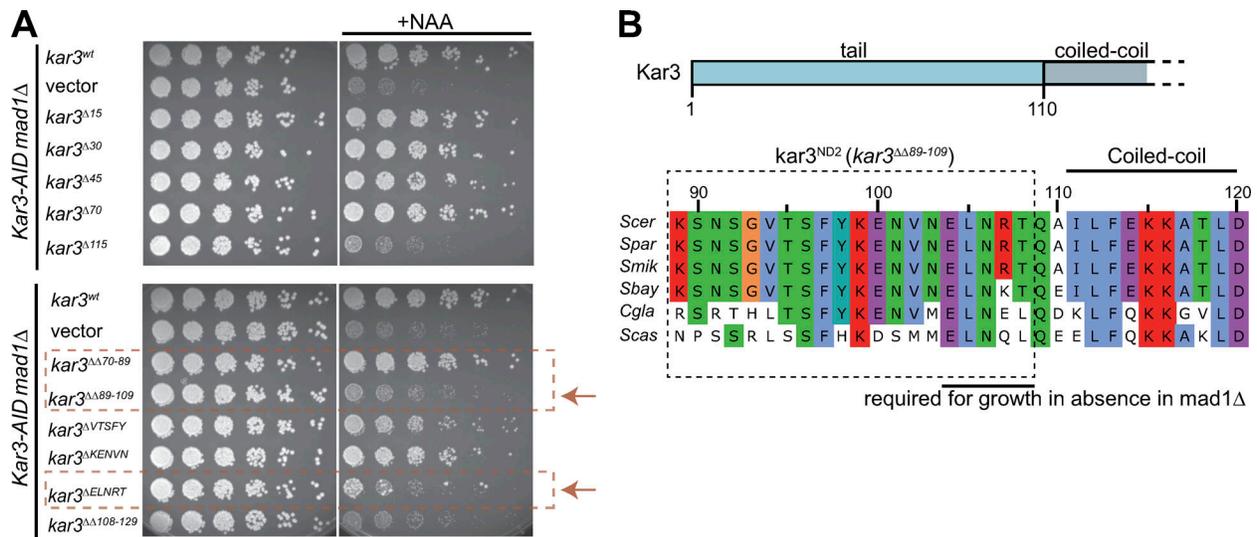
Figure S2. **Identification of key molecular elements in the Kar3 N-terminus. (A)** Kar3 mutagenesis screen. Different Kar3 rescue constructs were transformed into the Kar3-AID *mad1Δ* strain and tested for viability after depletion of endogenous Kar3 by the addition of auxin. Panels show N-terminal truncations (top) and finer mapping of critical regions close to a predicted coiled-coil as functionally important (bottom). Important mutants are highlighted with arrows and dashed rectangles. **(B)** Sequence alignment of the identified Kar3 sequence from six budding yeast species.
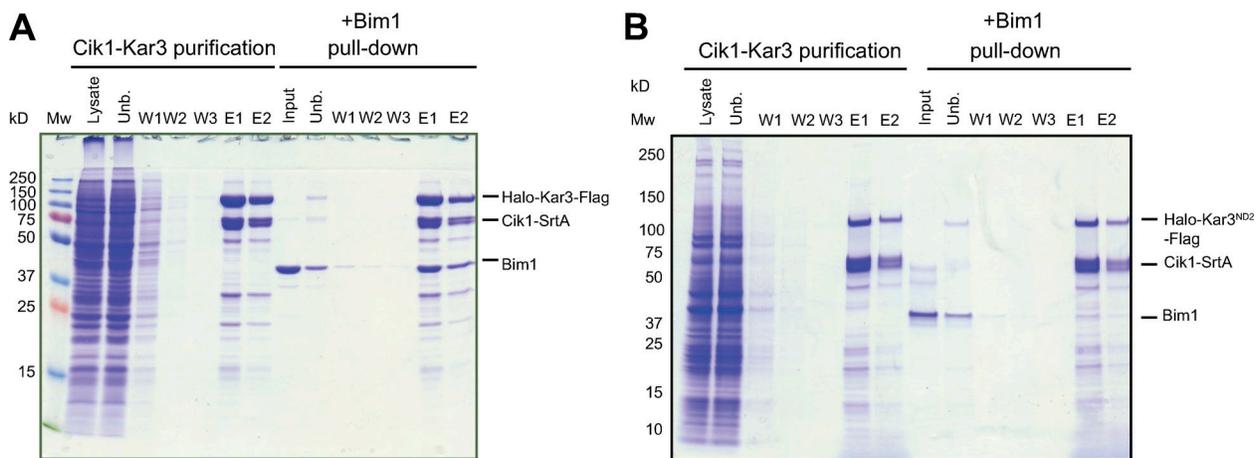
Figure S3. **Kar3ND2 mutants are defective in Bim1 binding. (A and B)** Purification and subsequent Bim1 pull-down experiment with Cik1-Kar3 wild-type (A) or Cik1–Kar3ND2 complex. Unb., unbound fraction. **(B)** Cik1–Kar3 complexes were purified from Sf9 extracts, bound to M2 agarose beads, incubated with Bim1, washed, and subsequently released from beads with 3× Flag peptide. Bim1 fails to copurify with the Kar3ND2 mutant.
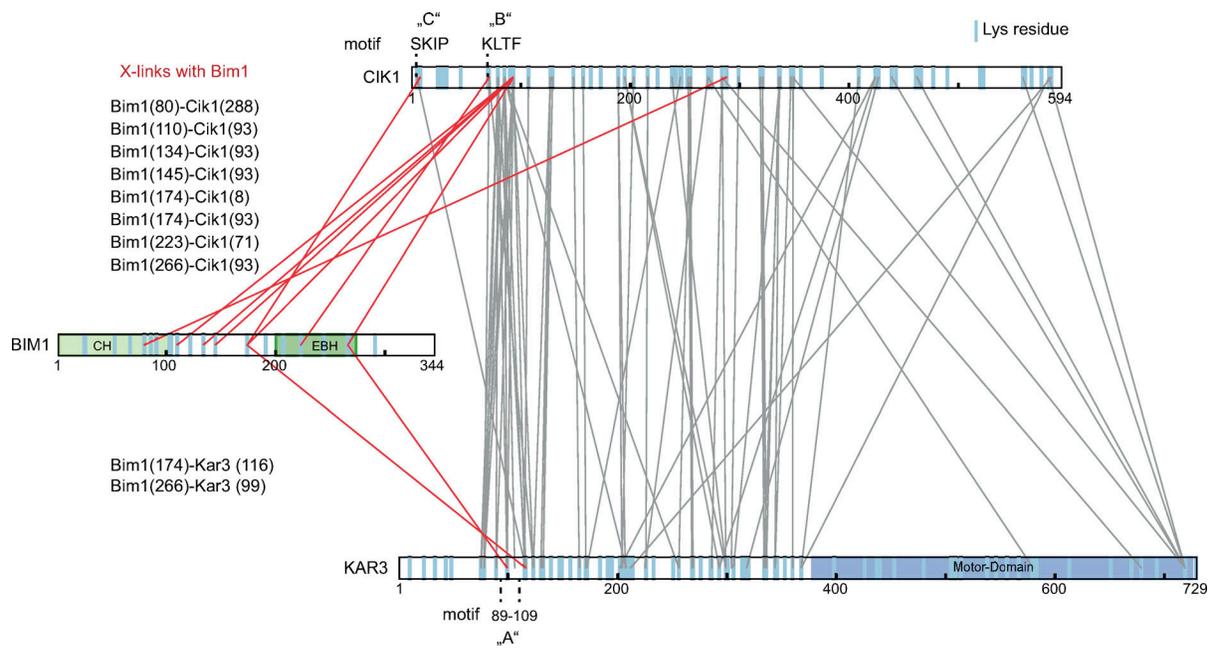
Figure S4.   **Relation between the identified binding motifs and the subunit topology of the Bim1–Cik1-Kar3 complex.** Display of chemical cross-linking data from (Molodtsov et al., 2016). Each line represents an individual Lys-Lys cross-link. Cross-links to Bim1 are highlighted in red and listed on the left. Numbers in parenthesis indicate the cross-linked lysine residue. The positions of Bim1-binding motifs A, B, and C are indicated; blue lines in the protein schemes denote all available lysine residues in the primary sequence.
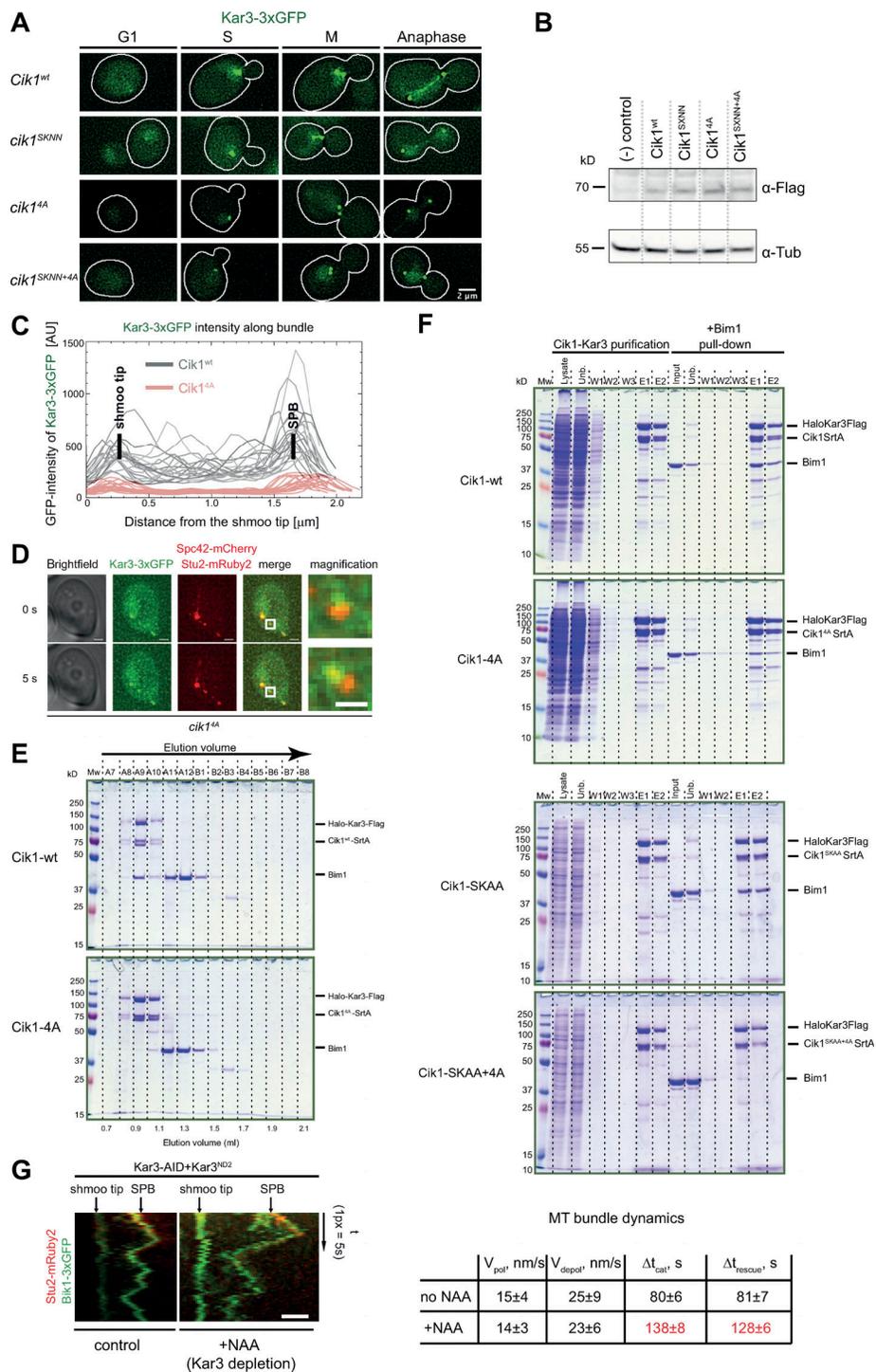
Figure S5. **Additional characterization of Cik1 mutants. (A)** Bim1 binding is required for an efficient association of Cik1-Kar3 with microtubule plus ends. Representative images show Kar3-3xGFP signals over different cell cycle stages in indicated Cik1 mutants. Cik1[SKNN]-Kar3 was still able to follow microtubule plus ends and bind to the metaphase spindle. The KLTF motif mutation abrogated plus-end localization. Scale bar is 2 µm. **(B)** Western blot analysis of Flag-tagged Cik1 rescue alleles. **(C)** Overlay of 15 line scans along the shmoo tip microtubule bundle of Kar3-3xGFP in Cik1[wt] and cik1[4A] genetic backgrounds. The KLTF motif mutation leads to a fourfold decrease in recruitment to the microtubule bundle. **(D)** Residual colocalization between Kar3-3xGFP and Stu2-mRuby2 in the Cik1-4A mutant. Microscopy images of two consecutive frames of α-factor–arrested cells are shown. Scale bar in panels 1–4 are 1 µm; scale bar for magnification is 0.5 µm. **(E)** Analytical SEC experiment showing that the Cik1-4A mutation in the KLTF motif prevents stable association between Cik1-Kar3 and Bim1. **(F)** Purification and subsequent Bim1 pull-down experiment with Cik1–Kar3 complexes containing either Cik1 wild type, Cik1-4A mutant, Cik1-SKAA mutant, or Cik1-SKAA+4A mutant. Note that only Cik1-SKAA+4A fully eliminates Bim1 binding in the pull-down assay. **(G)** Analysis of shmoo tip bundle dynamics in Kar3[ND2] cells. Kar3-AID cells expressing the Kar3[ND2] mutant and the plus-end markers Bik1-3xGFP and Stu2-mRuby2 were imaged in α-factor–arrested cells in the absence (control) and presence of auxin. Parameters of MT bundle dynamics are shown on the right; deviations from wild-type parameters are highlighted in red.

Video 1.   **Time-lapse epifluorescence microscopy of yeast cells expressing the microtubule-binding protein Bik1-3xGFP (green) and the SPB marker Spc42-RFP (red) in Cik1-AID cells.** OAI scans were taken every 10 min following synchronization of the cells with α-factor. Video shows cells under control conditions (no auxin added), corresponding to Fig. 2 A, upper panel (no aux). Video is displayed at 4 frames per second; scale bar is 2 µm. Fluorescence channels are merged with the corresponding bright-field images.

Video 2.   **Time-lapse epifluorescence microscopy of yeast cells expressing Bik1-3xGFP (green) and Spc42-RFP (red) upon depletion of Cik1-AID with auxin, corresponding to Fig. 2 A, bottom panel (plus aux).** OAI scans were taken every 10 min following synchronization of the cells with α-factor. Video is displayed at 4 frames per second; scale bar is 2 µm. Fluorescence channels are merged with the corresponding bright-field images. Note misorganization of microtubules on the nascent metaphase spindle at t = 10 min and 20 min, which eventually improves at t = 30 min.

Provided online are two tables. Table S1 lists yeast strains used in this study. Table S2 lists the relevant plasmids used in this study.